Describing hyperbolic surfaces with decorated tree graphs

and the relation to Weil-Petersson volumes

Author: Thomas Meeusen (s4822099)
Supervisor: Dr. T. Budd
Second reader: Dr. F.S. Saueressig

June 5, 2023

Abstract

To investigate JT gravity, a 2D quantum gravity toy model, previous approaches used recursion formulas to indirectly characterise relevant moduli spaces. Instead of using these recursion formulas we use a geometric approach. In this thesis, we investigate genus zero moduli spaces of hyperbolic surfaces with one marked cusp and a set of boundaries. We prove that we can associate a unique cut locus tree decorated with coordinates to each hyperbolic surface. These decorated cut locus trees prove to be useful in describing the moduli space (except for a subset with zero Weil-Petersson volume) as a bijection can be constructed between the two spaces. This space of decorated tree graphs is then combined with a new Poison algebra related to the inverse of the Weil-Petersson measure to derive the Euclidean measure. We investigate the use of the decorated tree graphs combined with the Euclidean Weil-Petersson measure as tools for JT gravity research. To test their use, we derived the string equation of hyperbolic surfaces with 2 marked cusps by using graph recursion and the Weil-Petersson measure, which agreed with other derivations. This shows that this approach can be used to derive entities in JT gravity, which will hopefully lead to a continuum limit of moduli spaces.

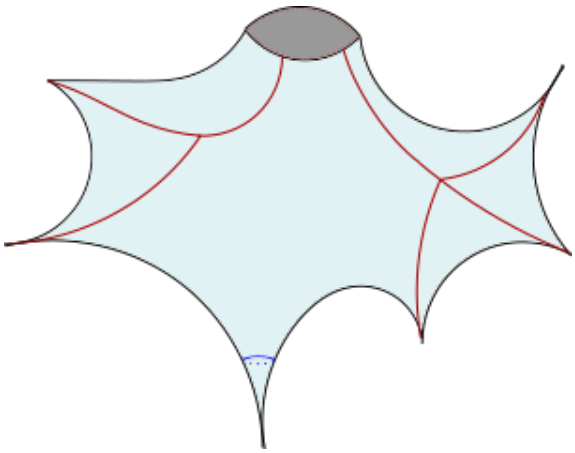

Figure 1: *An example of a hyperbolic surface with 6 cusps and a geodesic boundary of length $L > 0$. The red lines are the cut locus with respect to the bottom cusp whose horocycle is drawn in blue.*

Contents

1 Introduction

Mankind has always tried to explain and predict the phenomena of the world. Through science we have found ways of not only explaining the world around us, but also testing these explanations. In the realm of physics this ultimately led to two amazing theories: quantum field theory and general relativity. These theories have both been tested to an incredible precision. The gravitational red shift was measured with an uncertainty of only $7.6 \cdot 10^{-21}$ by scientists in Colorado in 2021 [1] and the quantum related fine structure constant α was measured in 2010 till 9 decimals making it the most precise experiment at the time [2]. These are just some of the ways the predictions of these two theories have been thoroughly tested and they are some of the best researched theories ever developed.

To further explain the world we often combined different scientific theories to build new ones. Electricity and magnetism, for example, were famously combined into the deeper theory of electromagnetism, which led us to the discovery that light is a form of electromagnetic radiation, leading to the invention of radio technology. Combining theories is not the only way to strengthen our understanding of a theory. Even deriving the same formula twice in different ways strengthens our understanding as the new tools can be used for other problems. Investigating the borders between different science fields has given new ways to reach a deeper understanding of the world.

In this quest for unification scientists were successful in combining almost all scientific theories. Quantum field theory and general relativity have however not yet been unified. In general relativity the geometry of space-time is connected to the energy within the space-time by $G_{\mu\nu} + \Lambda g_{\mu\nu} = \kappa T_{\mu\nu}$. Because the energy of space-time has quantum fluctuations from quantum field theory there should also be quantum fluctuations in the geometry of space-time. Therefore we need a new deeper theory that reproduces the old theories in a limit of, for example, high or low energy. This has led many scientists to the search for a Quantum Gravity Theory.

Quantum Gravity In the 1930-1940 the first scientists were already working on quantizing gravity, but it would take scientists till around the 1960s to start exploring the most promising paths of quantum gravity. An example of this attempt is to find a direct quantization of general relativity in 1963 [3]. This search for quantum gravity lead to three early researched branches of Quantum Gravity: treating G_N as a coupling constant, introducing a graviton particle and string theory. When we talk about directly quantizing gravity we mean treating the Einstein-Hilbert action $S = \frac{1}{16\pi G_N} \int \mathrm{d}^4x \sqrt{g}\mathcal{R}[g]$, where g is the metric of space-time and $\mathcal{R}$ is the Ricci scalar, in the same way as the action of other quantum theories with G_N as the coupling constant. Introducing the graviton to explain Quantum Gravity is a slightly different approach. Here a graviton G is introduced, which acts similarly to the W and Z bozons in the electroweak theory, but it would instead be the force carrier of gravity. Lastly string theory envisions 1 dimensional strings as the fundamental structures of the universe, which are wrapped up in interesting geometric configurations in hidden extra dimensions. The vibrations and configuration of these strings are then responsible for all

the properties of both General Relativity and Quantum Field Theory. These paths all have their own problems however. Directly treating G_N as a coupling constant in a quantum field theory has the problem that it has a negative mass dimension in 4-dimensions, meaning that the theory is non-renormalizable and one would need infinitely many measurements to get any prediction from the theory [4]. Introducing a graviton as a new force particle for gravity has similar problems and the theory is also non-renormalizable [5][1]. Lastly, string theory has been studied widely and is a mathematically beautiful way of describing Quantum Gravity, but it suffers from a lack of predictions that can be experimentally tested [6].

Many other paths have since been investigated, but so far scientists do not agree on any complete theory of quantum gravity. To solve this, some scientists are trying out more general geometric theories as a new approach. These theories revolve around different ways of solving a path integral of the form $Z = \int_{\text{metrics}} \mathcal{D}[g_{\mu\nu}] e^{S(g_{\mu\nu})}$ where $g_{\mu\nu}$ is a metric, S is an action like for example the Einstein-Hilbert action and $\mathcal{D}[g_{\mu\nu}]$ is a density for the metrics. The path integral is an integral over all possible metrics or geometries. If you try to do this integral without any restrictions it diverges because some geometries are equivalent to each other and they are counted multiple times, while they should only contribute once. The trick to doing the path integral is to first restrict yourself to a well defined subset of geometries, which you can calculate, and then taking a limit to retrieve the full space of geometries. This often involves quantizing a space-time with discrete blocks like triangles or simplices and then taking the continuum limit. In this limit the number of triangles goes to infinity, producing a manifold to hopefully recover all geometries, which can then lead to a quantum field theory of the metric or in other words a full Quantum gravity theory. Full 4-dimensional Quantum Gravity theories can be complex however and there is still a lot to learn in just 2-dimensional Quantum Gravity. Greater insight into 2-dimensional Quantum Gravity can give hints for new observables to test in 4D or what properties a 4-dimensional Quantum Gravity theory would have. In other words, understanding these 2D theories and their toy models can help guide our search for higher-dimensional quantum gravity theories.

2D Quantum Gravity To understand the 2D path integral we need some way of counting all the possible metrics in a controlled way. There are many ways to attempt this, two of which are relevant to this thesis: random triangulations and Jackiw[7]–Teitelboim[8] (JT) gravity. They both restrict the space of possible geometries to a simpler subset as an in between step to avoid divergences. The full space of geometries can then be recovered by taking a limit. These two approaches consider different types of subsets. JT gravity tackles continues surfaces with constant negative curvature while random triangulations discretizes the surfaces.

Within random triangulations you limit the geometries by approximating them with a gluing of flat triangles. The global structure and properties will then depend on how the

[1] There are ways to make gravitons work as a theory, like treating it with effective field theory, but gravitons in their simplest form do not work [5].

triangles are glued together. This way you can approximate many geometries by simply varying the way you create triangulation's. These descretized spaces can then be studied by doing simulations of random triangulation of finite size and measuring their geometric properties. This field of study investigates discreet finite surfaces and to recover all geometries in 2D you need to take a continuum where the number of triangles goes to infinity. This continuum limit of 2D gravity is called the Brownian sphere and shows up in multiple situations of 2D quantum gravity [9]. This Brownian sphere has many properties that make it useful in Matrix Models [10] and Liouville quantum gravity [11] and it is one of the great successes in 2D quantum gravity.

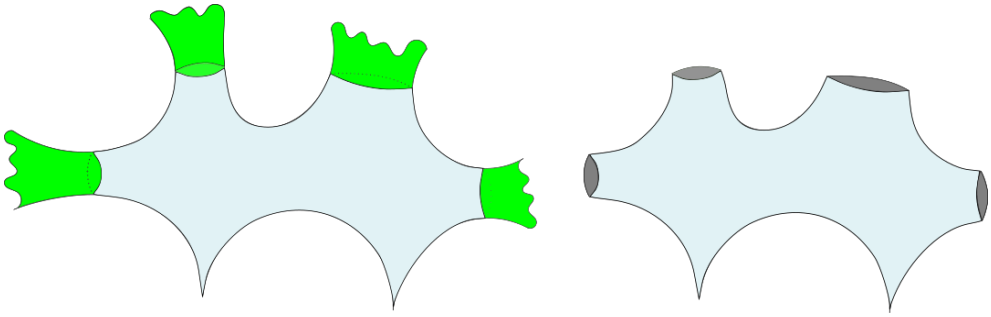

Figure 2: *An example hyperbolic surface split into the bulk (light blue) and trumpets (green). On the bottom the bulk of the hyperbolic surface is isolated.*

Instead of starting with discreet surfaces you can also start with surfaces with constant curvature. Here you have two choices: positive and negative curvature. The question is, why JT gravity deals with constant negatively curved spaces specifically[2]? The answer is that JT gravity is a 2D toy model that arises naturally when you try to include dilaton particles using scalar fields in the Einstein Hilbert action. It is governed by the classical action $J = -\frac{1}{2}\int_{\mathcal{M}} \sqrt{g}\phi(R+2) + J_{\text{Boundary}}$ [12], where ϕ is the dilaton field, g is the metric, R is the Ricci curvature, $\mathcal{M}$ is the full space-time and J_{Boundary} is the action of the Swarzian boundaries. Varying this action with respect to the dilation field simply gives the equation $R+2=0$, which explains why this theory is interested in negatively curved surfaces. Such a surface with a constant negative curvature is called a hyperbolic surface.

In JT gravity, scientists study collections of hyperbolic surfaces that are topologically equivalent to each other. These surfaces can then be split into two parts: the "trumpets" and the bulk moduli space as can be seen in Figure 2. The trumpets consider the contribution of the boundaries of the surface. Trumpets are hyperbolic surfaces with one geodesic boundary and one more complex Swarzian boundary, governed by the boundary action, while the bulk moduli space is the collection of hyperbolic surfaces with cusps and geodesic boundaries, governed by the bulk action. The Weil-Petersson form is a natural density to assign to each surface, which is well defined on these moduli spaces. This measure gives us a way

[2]There exist JT gravity theories with zero or positive curvature, but these are less common forms of JT gravity and they will not be considered in this thesis.

to compare the sizes of moduli spaces with each other and is found in different contexts [13]. The Weil-Petersson measure can be integrated over all surfaces in the moduli space to get the Weil-Petersson volume, which by construction is the full contribution of the moduli spaces in the JT gravity path integral [14]. These volumes allow us to calculate the path integral of JT gravity as they measure the contribution of the moduli spaces within JT gravity. The Weil-Petersson volume is also the contribution of these negatively curved surfaces with positively curved boundaries to the path integral.

If we can understand more properties of these moduli spaces we are better equipped to deal with the path integral. The Weil-Petersson volume of a general moduli space is one of these properties that is not understood well enough as there is still no unique formula for the Weil-Petersson volume with a general set of boundaries. To understand JT gravity better there are two ways of doing research, which use different tools. They tackle the same problems, but approach them from different sides. One approach uses algebraic analysis while the other uses direct geometric proofs. In algebraic analysis new properties of moduli spaces are derived by finding new algebraic solutions to the relevant equations. Meanwhile geometric derivations are done by directly investigating the hyperbolic surfaces and their structures. These two ways overlap and if possible scientists would like proofs in both approaches to further combine their respective tools. By exploring both research paths algebra can guide new geometric proofs and vice versa. An algebraic solution, for example might hint that there is a geometric property or a new method could tackle problems that were unsolvable before.

The surfaces in JT gravity are clearly just a subset of all possible geometries. To recover new geometries, more and more boundaries can be added, which balances the surfaces with positive and negative curvature. When we understand the moduli spaces well enough it would be interesting to look into a continuum limit of taking the number of boundaries to infinity to retrieve the full space of geometries.

With a continuum limit of moduli spaces we could connect JT gravity and the Brownian sphere directly allowing tools and results from the two fields to be applied to each other. One promising way to find a continuum limit of moduli spaces is to copy a derivation of the Brownian sphere. In this derivation of the Brownian sphere we start with a collection of random rooted graphs embedded on the sphere. Distance on this graph is then measured to the rooted vertex. Each vertex has a shortest path to the rooted vertex and the distance is then simply the number of steps on this path to the rooted vertex. Once you have this space of random graphs with a distance function on it the continuum limit is taken where the graphs become infinitely large. This is done by taking the size of the random graphs to infinity, which produces a random metric space that is the Brownian sphere. It is the one of the best studied continuum limit or universality class in 2D gravity and if we could connect JT gravity to it as well the fields could become even more interconnected. If we could find a way to generate graphs from moduli spaces we might be able to use the Weil-Petersson measure to encode distances on these graphs, by comparing geodesic distances from a cut

locus edge to a horocycle, which is already a couple of steps closer to the continuum limit of the moduli space.

Additionally if these Weil–Petersson measures have a simple form it could be used to find geometric derivations of the string equation[3] that arise from algebraic analysis. The string equation is a closed-form equation for the generating function of Weil-Petersson volumes (or grand-canonical partition function of JT gravity) with two marked cusps that uniquely determines the generating function. Many of the properties of the generating function can also be derived from the string equation.

In this thesis we investigate the connection between moduli spaces and tree graphs. We also investigate to which extent this new approach can be used to research moduli spaces geometrically and if this approach can lead to a continuum limit of Moduli spaces. We aim to describe the moduli spaces with these graphs to derive their Weil-Petersson measure. To test this new approach we will try to geometrically derive the string equation, which was originally derived algebraically. As a guide for that process we focus on the following research questions:

Research questions:

i Can we describe hyperbolic moduli spaces with decorated tree graphs?

ii Is there a direct geometric way of evaluating the JT gravity path integral?

iii Can decorated tree graphs and their Weil-Petersson measure be used to find a continuum limit of Moduli spaces?

To answer these questions I will describe a way to generate trees from hyperbolic surfaces in Section 3. This will give rise to a bijective function between subspaces of the moduli and graph spaces in Section 5. The connection between the Weil-Petersson measure and the Poison algebra will be investigated in Section 6. We will then use this bijection and the Poison algebra to derive the Weil-Petersson measure of the moduli spaces of genus zero in Section 6, which is then used to derive the string equation in Section 8.

[3]This string equation is not related to string theory.

2 Theory

This thesis uses many basic properties of hyperbolic geometry, topology and generating functions which will not be explained in the proof itself as it would slow down the pace of the story. Not everyone is familiar with these topics however, so in this section I will give some of the basic theory in the fields we will use in this thesis. Feel free to skip this section if you are familiar with hyperbolic geometry, moduli spaces, Weil-Petersson volumes, topology and generating functions. If that is not the case this chapter will hopefully help you to understand some of the basics in these subjects.

2.1 Hyperbolic Surfaces

The central objects within this thesis are hyperbolic surfaces. As mentioned before JT gravity uses hyperbolic surfaces extensively, but what are hyperbolic surfaces? To work with hyperbolic surfaces we first need to know how properties of curved spaces are different from flat geometry and how they came to be. To do that, we need to go back in time.

All the way back in 300BC Euclid compiled 5 postulates from which all of geometry at the time could be derived.

1. A straight line (or geodesic) may be drawn between any two points.
2. Any terminated straight line may be extended indefinitely.
3. A circle may be drawn with any given point as center and any given radius.
4. All right angles are equal.
5. *For any given point not on a given line, there is exactly one line through the point that does not meet the given line.*

The 5^{th} postulate was however controversial because the statement is not self evident like the others. It turns out that this 5^{th} postulate is the only postulate that is not true for curved spaces. In hyperbolic geometry there is not just one line for the 5^{th} postulate, but infinitely many. This means that many of the proofs of geometry are still applicable in curved spaces, but some no longer hold. For example a "straight line" or geodesic between two points is still locally the shortest path, but there are no rectangles in hyperbolic geometry as the angles can't all be $\pi/2$. In this section I will discuss some of the properties that are different or completely new in hyperbolic geometry.

But how do we define a hyperbolic surface if we keep these properties in mind? A hyperbolic surface is a 2-dimensional surface with constant negative Gaussian curvature $K = -1$ and scalar curvature $R = 2K = -2$. The Gaussian curvature of -1 is by convention as other curvatures just zoom in or out on the surface. A part of a hyperbolic surface is shown in Figure 3 to illustrate this negative curvature.

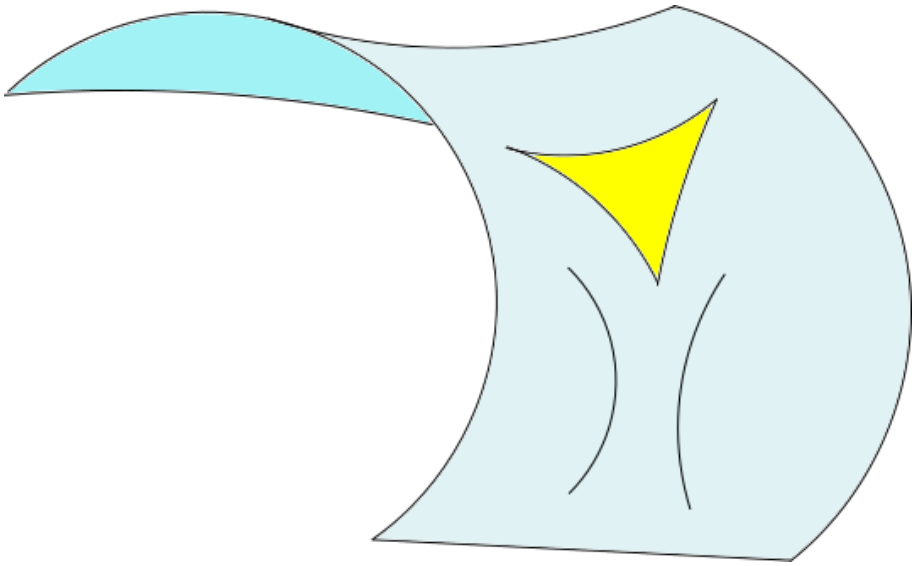

Figure 3: *A part of a hyperbolic surface with a hyperbolic triangle in yellow. Two geodesics are shown in black on the surface.*

One way to characterize surfaces is by dividing them into triangles. You can easily see how you could divide the flat plane or a piece of paper into triangles. The same concept can be used for hyperbolic surfaces, but we will need to define what a triangle is in hyperbolic geometry and we need to know what properties they have. We are all familiar with flat triangles, but some basic properties of triangles do not hold in curved spaces. We will use these triangles extensively in this thesis, so let's investigate their properties.

A triangle consists of 3 vertices and 3 geodesic lines connecting them. This definition still works in hyperbolic geometry, but there are a few differences with the Euclidean triangle. Because of the curved nature of the hyperbolic surface, the angles a, b, c of a hyperbolic triangle add up to $a + b + c < \pi$. This is because the lines bend away from each other in hyperbolic geometry and to compensate the angles must be smaller. A triangle in hyperbolic geometry is even completely determined by the angles of the triangle. This is because a larger triangle means the lines are more curved and thus produce even smaller angles and so each set of angles has exactly one triangle associated to it. The area of a hyperbolic triangle is directly related to the angles by $A = \pi - (a + b + c)$ and an example hyperbolic triangle is shown in Figure 3.

To compare and identify triangles it is useful to learn about the types of similar and congruent triangles in hyperbolic geometry. We use the convention SAS that refers to side, angle, side, where the order is important here as the angle is enclosed by the pairs of sides. This notation can then be used for other combinations of shared side lengths or angles ASA, two angles on both sides of a side, AAA for similar triangles, etc. Two triangles are congruent in hyperbolic geometry if they share: AAA, SAS, ASA, SAA, SSS.

Because the area of a hyperbolic triangle is $\pi - (a + b + c)$ there is a largest unique triangle called an ideal triangle with angles $a, b, c = 0$. The sides of these triangles are infinitely long.

Any point that is infinitely far away on a hyperbolic surface is called an ideal point. There is however a way to give a distance measure to the sides of an ideal triangle. For an ideal point one can define a so called horocycle as a curve where all perpendicular geodesics converge at the ideal point. If this is done for each ideal point the distance between horocycles and to horocycles is well defined.

2.1.1 Hyperbolic projections

Just like it is useful to have a flat map of the earth it is also often useful to map the hyperbolic plane to a flat 2D surface. The two projections that we will use in this thesis are: the Poincaré half-plane and the Poincaré disk.

In the Poincaré half-plane projection the hyperbolic surface is projected to the upper half of the complex plane. The geodesic lines in this projection are half circles with their center on the real axis. Vertical lines are also geodesics as they correspond to a half circle of infinite radius. The metric that determines the distances on this half-plane is

$$(\mathrm{d}s)^2 = \frac{(\mathrm{d}x)^2 + (\mathrm{d}y)^2}{y^2}.$$

The hyperbolic distance between points $p_1 = x_1 + y_1 i$, $p_2 = x_2 + y_2 i$ are then measured along these half circles and are given by

$$\begin{aligned} \mathrm{dist}(p_1, p_2) &= 2\mathrm{arsinh}\left(\frac{||p_2 - p_1||}{2\sqrt{y_1 y_2}}\right) \\ ||p_2 - p_1|| &= \sqrt{(x_1 - x_2)^2 + (y_1 - y_2)^2} \\ \mathrm{dist}((x, y_1), (x, y_2)) &= \ln\left(\frac{y_2}{y_1}\right). \end{aligned}$$

From this distance calculation we can conclude that the ideal points in this projection are any points $(x, 0)$ or (x, ∞) $\forall x \in \mathbb{R}$, as they are infinitely far away from all other points. Horocycles are circles that touch the real axis for an ideal point on the real axis or horizontal lines for an ideal point at infinity. With these properties in mind an ideal triangle can be easily drawn in the half-plane, as shown in Figure 4.

In the Poincaré disk projection the hyperbolic plane is projected onto a disk. The ideal points are the points on the boundary of this disk. Geodesics are circles that meet the boundary at right angles. An example of an ideal triangle in this projection is shown in Figure 5.

Sometimes we will need to glue two triangles together in these projections to create hyperbolic surfaces. There is a degree of freedom in how you glue two infinite sides of a

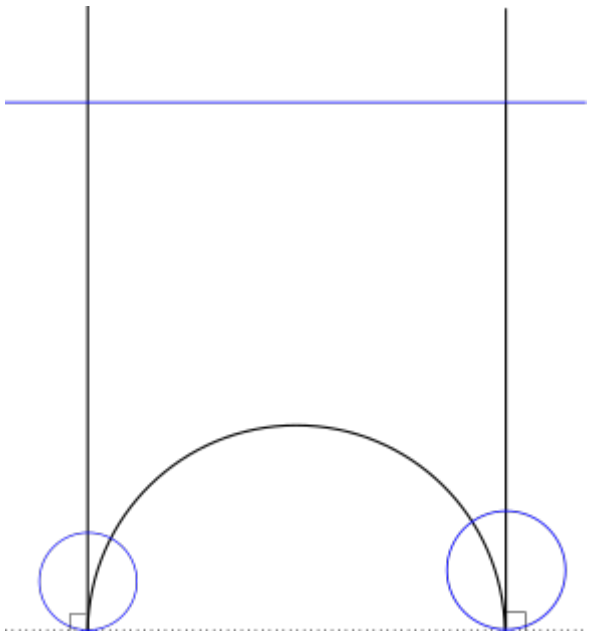

Figure 4: *An ideal triangle in the upper half-plane projection. The blue lines are the horocycles and the dotted line is the real axis. Because the sides of the triangle are geodesics they meet the real axis at a right angle.*

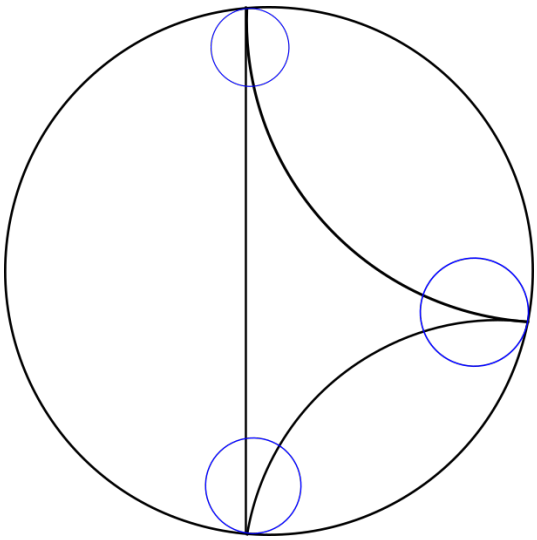

Figure 5: *An ideal triangle in the Poincaré disk. Horocycles are included for each of the vertices of the triangle in blue.*

triangle together as they can be shifted with respect to each other. We can remove this uncertainty by using Möbius transformations to make sure that two sides of a triangle are equivalent. This is because Möbius transformations are the isometries of the hyperbolic planes. Isometries are also known as congruent transformations, because two shapes are congruent if there is an isometry that sends one geometric shape to the other. So, if two sides are related by an isometry they are congruent and can be identified as the same edge. These isometries in the halplane model complex plane are of the form

$$f(z) = \frac{az + b}{cz + d},$$

where $z = x + iy$ for (x, y) in the Poincaré half-plane and $a, b, c, d \in \mathbb{R}$.

2.1.2 Hyperbolic Boundaries

The hyperbolic surfaces in this thesis include boundaries, which are points in the closure, but not in the interior of the surface. These come in two varieties: cusps and geodesic boundaries. Cusps are single points at infinite distance, and any two geodesics, that end at the same cusp, converge to each other.

Geodesic boundaries are geodesics, that loops back to themselves, where the surface ends. These boundaries have a well defined length, which is just the length of the boundary geodesic. In the limit where this length goes to zero the boundary becomes a cusp. These boundaries distinguish different moduli spaces from one another and many of their properties are determined by the boundaries. We will also use the convention that a boundary of length $L = 0$ corresponds to a cusp.

2.2 Topology

For this thesis we study hyperbolic surfaces that are similar to each other in their general shape. Therefore it would be nice to have some general properties that still hold if there are only continuous deformations. This is what topology is all about.

Topology is the study of surfaces under continuous deformations. The most famous example is that you can deform a donut continuously into a coffee cup, which illustrates that two very different geometries can be homeomorphic. Such a continuous deformation is called a homeomorphism. If two surfaces have a homeomorphism between them they are called homeomorphic or topologically equivalent and they share topological properties.

To make this more concrete let's define what we mean with a homeomorphism. A homeomorphism is a bijective continuous function with a continuous inverse. A function within topology is continuous if the inverse of any open set is also an open set.

One homeomorphism we will use is a retraction. This is a continuous mapping of a set H onto a subset $Q \subset H$ such that the retraction preserves the position of the points already in Q. The relative position is determined by looking at the distance of the shortest path to the subset.

Figure 6: *An example of a transparent cube.*

In general it can be quite hard to find a homeomorphism. Luckily there is an easier way to check if two surfaces with the same number and type of boundaries are homeomorphic: the Euler characteristic. The Euler characteristic is a topological invariant and additionally two orientable surfaces are homeomorphic if they have the same boundaries and the same Euler characteristic. For a polyhedron it is defined as $\chi = V - E + F$ where V, E and F are the number of vertices, edges and faces of the surface respectively. For a cube like in Figure 6 for example you can simply count the number of faces, edges and vertices of a cube: $V = 8, E = 12, F = 6$, the Euler characteristic is then $\chi_{\text{cube}} = 2$. Our surfaces are continuous, but we can still use this relation by triangulating our surfaces and counting the resulting number of faces, edges and vertices.

This work has already been done by others as the Euler characteristic for our surfaces is known if we know the genus and the number of boundaries of our surfaces. The genus of a surface is the number of handles in the surface. Without going into the exact details we can intuitively tell that a donut has one handle and has genus 1 while the sphere has zero handles and genus 0. Then the Euler characteristic is $\chi = 2 - 2g - b$ where b is the number of boundaries and g is the genus [15].

The projections we discussed in Section 2.1.1 are universal covers of a hyperbolic surface meaning we can use many of the topological properties in this section. The universal cover of a simply connected topological space H is a simply connected space Y with a surjective open map $f : Y \to H$ that is a local homeomorphism.

The last concept we need to introduce is the concept of homotopy classes of curves. If a curve can be continuously deformed into another curve we say that these curves are in the same homotopy class. These homotopy classes have certain properties that we will use later in this thesis.

2.3 Moduli Spaces

In this thesis we work with moduli spaces of genus 0 with one marked cusp called the origin, but before we can start describing what a moduli space is we first need to define the Teichmüller space of a hyperbolic surface $\Sigma_{g=0,n+1}$ $\mathcal{T}_{g=0,n+1}(\mathbf{L})$ [16]. For an n-tuple $\mathbf{L} = (L_1, L_2, ..., L_n)$ of positive real numbers, let the hyperbolic surfaces in $\mathcal{T}_{g=0,n+1}(\mathbf{L})$ be

the set of hyperbolic surfaces H of genus $g = 0$ with n geodesic boundary components, whose lengths are prescribed by $\mathbf{L}$, and a marked cusp called the origin. Each of these hyperbolic surfaces is combined with a label fixing homeomorphism $f_H : \Sigma \to H$ where the length of the boundaries L_i is left invariant under f_H. This means only those surfaces H with a label fixing homeomorphism to Σ are included in the Teichmüller space. These hyperbolic surfaces H and the functions f_H together form the Teichmüller space

$$\mathcal{T}_{g=0,n+1}(\mathbf{L}) = \left\{ (H, f_H) \;\middle|\; \begin{array}{l} H \text{ is a hyperbolic surface of genus 0 with} \\ \text{one marked cusp and boundary components} \\ \beta_1, \beta_2 ... \beta_n \text{ of lengths } L_1, L_2, ..., L_n \text{ and} \\ f_H : \Sigma \to H \text{ a label-fixing homeomorphism} \end{array} \right\} \sim . \quad (1)$$

In this case, $(H_1, f_1) \sim (H_2, f_2)$ if and only if $f_2 \circ f_1^{-1}$ is an embedding homotopy that also conserves distances. These equivalent classes are all homeomorphisms, which preserve the labeling of the boundaries. Alternatively you can see the Teichmüller space as the collection of metrics with Ricci scalar $R = -2$ on a surface with genus 0, modulo small diffeomorphisms isotopic to the identity. These homeomorphisms can be split into two groups, those that are equivalent to the identity on $\mathcal{T}_{g=0,n+1} : (\mathbf{L})$ $\text{Homeo}_0(\Sigma)$ and those that are not: $\text{Homeo}(\Sigma)$. We do not want to include $\text{Homeo}_0(\Sigma)$ in the equivalence relations of the moduli space. To do this lets define the equivalence mapping class group of the moduli space $\text{Mod}(\Sigma) = \text{Homeo}(\Sigma) \setminus \text{Homeo}_0(\Sigma)$. Then we will restrict ourselves to the moduli space $\mathcal{M}_{g=0,n+1}(\mathbf{L}) = \mathcal{T}_{g=0,n+1}(\mathbf{L}) \setminus \text{Mod}(\Sigma)$, which excludes these identity equivalence relations. Thus, the moduli space is

$$\mathcal{M}_{g=0,n+1}(\mathbf{L}) = \left\{ H \;\middle|\; \begin{array}{l} H \text{ is a hyperbolic surface of type (g=0, n+1) with} \\ \text{one marked cusp and boundary components} \\ \beta_1, \beta_2 ... \beta_n \text{ of lengths } L_1, L_2, ..., L_n \end{array} \right\} \sim, \quad (2)$$

where two hyperbolic surfaces $H_1 \sim H_2$ if they are isometric, meaning there is a distance preserving transformation between them.

Thus the moduli space is a collection of hyperbolic surfaces with an equivalence relation. This space includes many different hyperbolic surfaces, so to count their contribution to the path integral we need some way of measuring the dimension of the moduli space. To find the dimension of the moduli space it helps to split the hyperbolic surfaces into smaller parts we can easily describe. These smaller parts are called pairs of pants.

2.3.1 Pair of pants decomposition

A pair of pants is a hyperbolic surface with 3 labeled geodesic boundaries of lengths L_1, L_2, L_3. It turns out that such a hyperbolic surface is uniquely defined [16]. If we can split a larger surface into pairs of pants and then glue them back together uniquely we can recover the full moduli space by just studying how to glue pairs of pants together. You can split a hyperbolic surface into pairs of pants with a maximal collection of disjoint

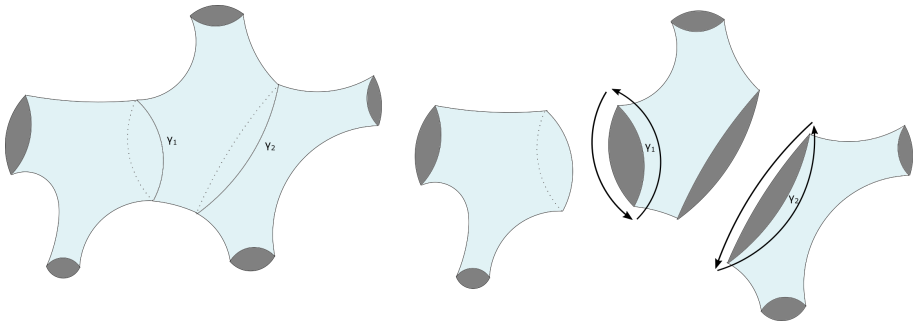

Figure 7: *The pants decomposition of an example hyperbolic surface with 5 boundaries into three pairs of pants. The geodesics γ_1, γ_2 are shown as black lines with dotted lines for parts of the geodesic on the back.*

simple closed geodesics $\gamma_1 ... \gamma_{n-2}$ on the surface and cutting along them as can be seen in Figure 7. This splits a surface with $n+1$ boundaries into $n-1$ pants. To recover the full hyperbolic surface we need know two things. What are the lengths of these geodesics γ_i so we can uniquely determine each pair of pants and how do we glue them back together. The length of the geodesics is self explanatory, but what do we need to know to glue two geodesics together?

When you glue two geodesics together you can first rotate the geodesics before gluing them together, so you need to know how much the two geodesics are rotated with respect to each other. Thus to recover the full hyperbolic surface we need the lengths l_i of the geodesics γ_i and the twist parameter $\tau_i \in [0, l_i)$. These are called the Fenchel-Nielsen coordinates and for each γ_i there are 2 Fenchel-Nielsen coordinates. With this we can immediately see that the dimension of our moduli space $\mathcal{M}_{g=0,n+1}(\mathbf{L})$ is $2(n-2)$.

We can now describe the moduli space better, but we still need a way to calculate its contribution to the path integral. For this we need to know what Weil-Petersson volumes are. The Fenchel-Nielsen coordinates are useful to illustrate the Weil-Petersson volumes, but they are not particularly useful for describing moduli spaces with tree graphs.

2.3.2 Weil-Petersson volumes

As mentioned before the Weil-Petersson volume of a moduli space encodes the contribution of the bulk in the JT gravity path integral. To construct the Weil-Petersson volume we have three steps, which will be illustrated in the Fenchel-Nielsen coordinates. First we start with the Weil-Petersson symplectic form on the Teichmüller space [17]

$$\omega_{WP} = \sum_{\alpha \in \mathcal{P}} \mathrm{d}l_\alpha \wedge \mathrm{d}\tau_\alpha. \tag{3}$$

The volume form is then the product of this Weil-Petersson form defined as

$$\mathrm{d}\mu_{WP} = \frac{1}{(n-2)!}(\wedge \omega_{WP})^{n-2}. \tag{4}$$

This volume form can then finally be used to define the Weil-Petersson volume

$$V_{g,n+1}(0, L_1, ..., L_n) = \int_{\mathcal{M}_{g,n+1}} \mathrm{d}\mu_{WP}. \tag{5}$$

Although this definition is not too complex, actually calculating the Weil-Petersson volumes directly is quite difficult. This is normally done by applying Mirzakhanis recursion identities [16].

2.4 Generating Functions

A generating function is a way of encoding an infinite series a_n by treating them as the coefficient of a power series. This seems like a rather strange way of encoding a series, but it proves to be a useful tool to find many useful properties of infinite series [18]. The generating function $G(x)$ of the series a_n is

$$G(x) = \sum_{n=0}^{\infty} a_n x^n.$$

A simple example of a generating function is the constant series $a_n = 1$. Then the generating function is simply the geometric series $\frac{1}{1-x}$. This illustrates that their are simple functions, which are also generating functions. We can start with an explicit generating function and try to find the coefficients a_n or try to find recursive relations of the function.

Exponential generating functions are also useful in combinatorics. One of the properties that makes them useful in combinatorics is that they work really well under differentiation. A exponential generating function E of a series a_n is equal to

$$E(x) = \sum_{n=0}^{\infty} a_n \frac{x^n}{n!}.$$

When differentiating this series you simply remove a_0 and shift all the other a_n in the series one place. If we differentiate repeatedly we find the useful property: $\frac{d^k}{d^k x} E(x)|_{x=0} = a_k$.

In general, generating functions are powerful tools to calculate statistical properties like averages, find recursive relations and prove many other properties of a series a_n. In this thesis we are specifically interested in the exponential generating function of the Weil-Petersson volumes R and if it has any recursive relations.

With this context on hyperbolic spaces, topology and generating functions we can get into the meat of this thesis.

3 Defining a unique cut locus tree from a hyperbolic surface

We want to investigate the connection between the moduli space $\mathcal{M}_{g=0,n+1}(\mathbf{L})$ and tree graphs to get closer to a possible continuum limit. To start we use the definition of Section 2.3 for the moduli space

$$\mathcal{M}_{g=0,n+1}(\mathbf{L}) = \left\{ H \;\middle|\; \begin{array}{l} H \text{ is a hyperbolic surface of type (g=0, n+1) with} \\ \text{one marked cusp and boundary components} \\ \beta_1, \beta_2 ... \beta_n \text{ of lengths } L_1, L_2, ..., L_n \end{array} \right\} \sim, \qquad (6)$$

where two hyperbolic surfaces $H_1 \sim H_2$ if they are isometric, meaning there is a distance preserving transformation between them. With this definition we can start creating some tree graphs using the cut locus. The cut locus of a point x in a Riemannian manifold is defined as all points on the manifold that have multiple shortest (geodesic) paths to the point x. In hyperbolic geometry this notion can be generalised to the shortest path to a horocycle, which in our case will be the horocycle of the marked cusp or origin. This is done by defining a horocycle for the origin and measuring distances with respect to the horocycle of the origin. An example of a point with one unique path is shown in Figure 8a and a point with two unique paths is shown in Figure 8b. Whether a point u in the manifold has multiple shortest paths is independent on the length of the horocycle as long as the horocycle does not encompass the point u. This means that for every hyperbolic surface with a marked cusp, one can choose a horocycle small enough such that the cut locus is uniquely defined.

To understand how the cut locus can lead to a tree structure we will first need to understand more of its properties. For this we will generalise lemma 2.2.1 from a paper [15]. This paper did not allow for boundary components of length $L_i > 0$. In addition the paper allowed for multiple marked cusps, which we will not look at here. We will repeat a slightly modified and expanded proof here that uses parts of the proof of lemma 2.2.1 of the paper. The proof in this thesis also uses different techniques that work only in our updated situation.

First we define a few things. Our hyperbolic surface $H \in \mathcal{M}_{g=0,n+1}(\mathbf{L})$ has one marked cusp, which we call the origin, with a horocycle of length c_0. As mentioned before the resulting cut locus will be independent on the choice of c_0 as long as it is sufficiently small. Let the area enclosed by this horocycle that contains the marked cusp be Ω, or the cusp area of the origin. The boundaries of length $L > 0$ we will simply call the boundaries $\beta_i \in \mathbf{B}$ and we will attach hyperbolic cylinders HC_i to them to continue the surface into infinity. Let $\mathbf{C}$ be the collection of unmarked cusps. Let P be the union of $\mathbf{C}$ and all the hyperbolic cylinders HC. For ease of notation, let $K = |\mathbf{K}|$ be the number of elements in a set $\mathbf{K}$ for any set **marked in bold**.

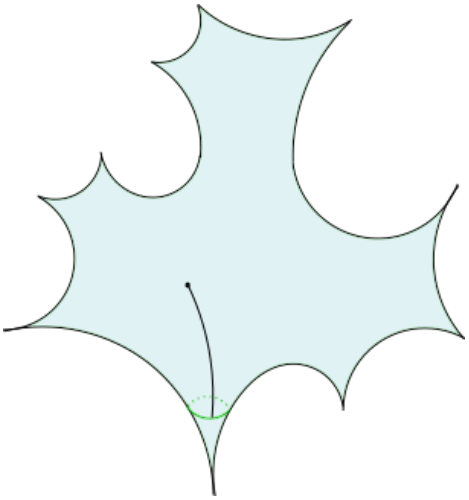

(a) *A point on a hyperbolic surface with one shortest path in black to the horocycle shown in green.*

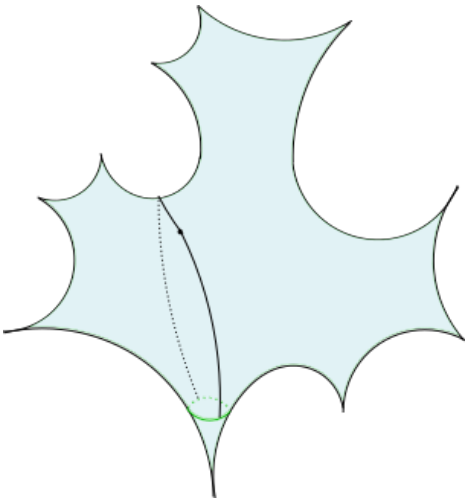

(b) *A point on a hyperbolic surface with two shortest paths in black to the horocycle shown in green. The dotted line represents a geodesic on the back of the surface.*

Figure 8: *Number of shortest paths for two points on a hyperbolic surface with 9 unmarked cusps and the origin.*

Given any point $u \in H \setminus P$ let w(u) be the number of shortest geodesics to Ω. Let $\Sigma = \{u | w(u) \geq 2\}$ and let $\mathbf{V} = \{u | w(u) \geq 3\}$. With these definitions we can modify lemma 2.2.1 of the paper to:

Lemma 1. *The function w(u) has the following properties:*

i w *is a locally finite, positive, integer valued function on* $H \setminus P$.

ii $\boldsymbol{V}$ *is a finite set of points.*

iii $\Sigma \setminus \boldsymbol{V}$ *consists of a finite union of open geodesic arcs. Each endpoint of an arc is either a cusp in* $\boldsymbol{C}$*, a boundary in* $\boldsymbol{B}$ *or a point in* $\boldsymbol{V}$.

iv Each cusp in $\boldsymbol{C}$ *and each boundary in* $\boldsymbol{B}$ *is an endpoint of at least one arc of* Σ.

v Each point in $\boldsymbol{V}$ *is at the head of at least three directed arcs of* Σ.

vi If we view multiple arcs of $\Sigma \setminus \boldsymbol{V}$ *entering a boundary in* $\boldsymbol{B}$ *as meeting in a single point, then* Σ *is fully connected and contains no loops.*

Proof. Take the universal cover of $H \setminus P$ to be the Poincaré disk. If c_0 is sufficiently small the horocycle of the origin consists of an infinite number of disjoint horodisks in the universal cover. Given $u \in H \setminus (\Omega, P)$ we lift it to the universal cover. There is a maximal

hyperbolic disk with center u whose interior is disjoint from Ω, as shown in Figure 9. Any given finite disk in the hyperbolic plane can only meet a finite number of disjoint horocycles in the universal cover. This means that w(u) is a finite positive integer for each $u \in H \setminus P$ and it is locally finite.

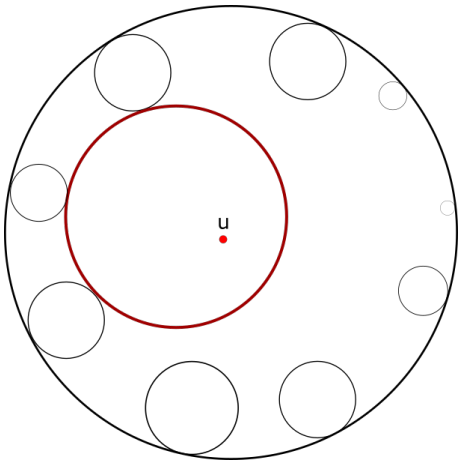

Figure 9: *The Poincaré disk with the horocycles of the origin shown in black. The large red circle is the largest possible disk that does not overlap with any horocycle and with center u.*

To investigate the shape of $\Sigma \setminus \mathbf{V}$ we look at two disjoint horocycles in the hyperbolic plane, as shown in Figure 10. The geodesic that joins the two centers of the horocycles has a section that is outside the horocycles, which has a midpoint m. Reflecting one horocycle with respect to the geodesic that is orthogonal in point m results in the other horocycle. This means that the orthogonal geodesic is the line equidistant between the two horocycles. This orthogonal geodesic is then an arc of $\Sigma \setminus \mathbf{V}$, that can continue to infinity or continue till another horocycle is equally close as the other two resulting in a point $v \in \mathbf{V}$. This means that $\Sigma \setminus \mathbf{V}$ consists of a union of geodesic arcs, which end in $\mathbf{V}$, end in a cusp in $\mathbf{C}$ or crosses a boundary in $\mathbf{B}$.

To see how many geodesic arcs there are in $\Sigma \setminus \mathbf{V}$, we isolate all cusps with new horocycles $c_1 ... c_i$. If you define small enough horocycles for each cusp $p \in \mathbf{C}$ and remove the corresponding cusp regions and hyperbolic cylinders from H the resulting surface H' will be finite. This means that a finite distance D exists such that for all points $u \in H'$ the distance to the marked horocycle $d(u) \leq D$. Any disk with a center on the marked horocycle and radius D can then only meet or intersect a finite number of disjoint horocycles of the origin in the hyperbolic plane and it includes all points in $H' \setminus \Omega$. Because the cusp regions are isolated they do not contain the marked horocycle, which means they do not contribute any extra marked horocycles of the origin. As a result only a finite amount of horocycles contribute to Σ and $\Sigma \setminus \mathbf{V}$ consists of a finite set of geodesic arcs. For the rest of this proof we will again limit ourselves to one horocycle around the origin and no horocycles for the

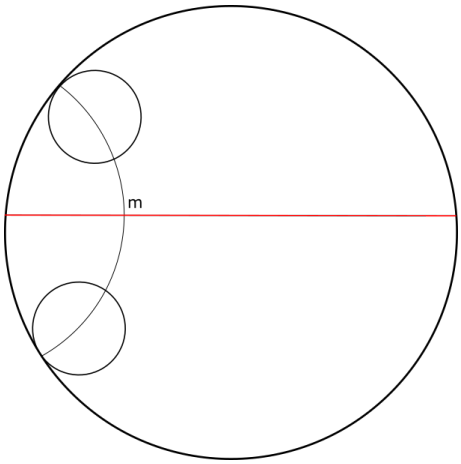

Figure 10: *Two disjoint horocycles with the geodesic that joins their centers. The red line is the geodesic line that is orthogonal to that geodesic in point m and is equidistant to both horocycles.*

other cusps.

To investigate the local structure of Σ let d_u be the distance of $u \in \Sigma$ to the nearest horocycle. The disk of radius d_u meets a finite set of horocycles F. The next nearest horocycle will have a distance $d_u + \epsilon$ to u. We can then define N as the disk of radius $\epsilon/2$ around u. For all points in N the closest horocycles will be in F because of the triangle inequality. This means that $\Sigma \cap N$ is fully determined by the horocycles in F and it has the form of $|F| \geq 2$ geodesic arches that meet in u, as shown in Figure 11. From this we know that $\mathbf{V}$ is a discrete closed set, that Σ is closed and that $\Sigma \setminus \mathbf{V}$ and $\mathbf{V}$ are locally finite.

This means that for each point $u \in \mathbf{V}$ at least 3 geodesic arcs meet. Because $\Sigma \setminus \mathbf{V}$ consists of a finite amount of geodesic arcs, $\mathbf{V}$ must also be finite. Now that we have determined most of the local structure we can look at what happens near the cusps and boundaries.

For each point $u \in H \setminus (\Sigma, \mathbf{C})$ there is only one shortest path to Ω. We can project $H \setminus (\Sigma, \mathbf{C})$ to the upper half-plane easily, as shown in Figure 12. Let h be the y coordinate of the horocycle in this projection. If we shift each point u by ih to u' they are all enclosed by the horocycle. This means that all the points in $H \setminus (\Sigma, \mathbf{C})$ can be retracted uniquely to Ω and that the two spaces are topologically equivalent. This is why $H \setminus (\Sigma, \mathbf{C})$ has the topology of a disk with one marked point, which has one outer boundary, because that is the topology of a disk with one marked point.

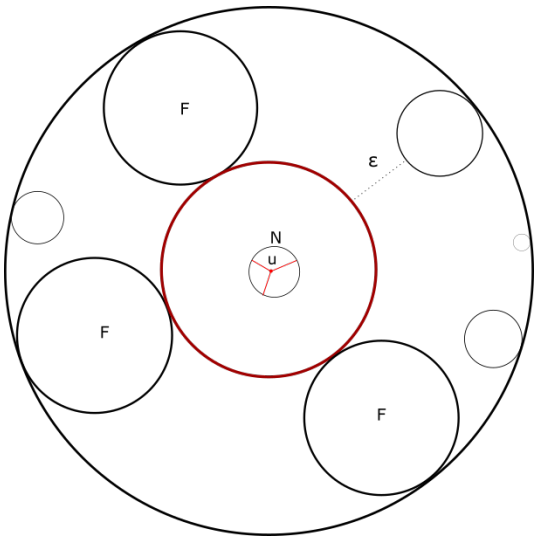

Figure 11: *The local structure of the cut locus in the Poincaré disk. The circles that touch the boundary of the Poincaré disk are horocycles. The red circle is the largest geodesic disk with centre u that only touches the horocycles. The horocycles marked with F are the ones that touch the largest disk. $\epsilon > 0$ is the distance between the largest disk and the next closest horocycle. The circle marked with N is the disk of radius $\epsilon/2$ around u. The cut locus is drawn in N and is made up of 3 geodesic arches that meet in u.*

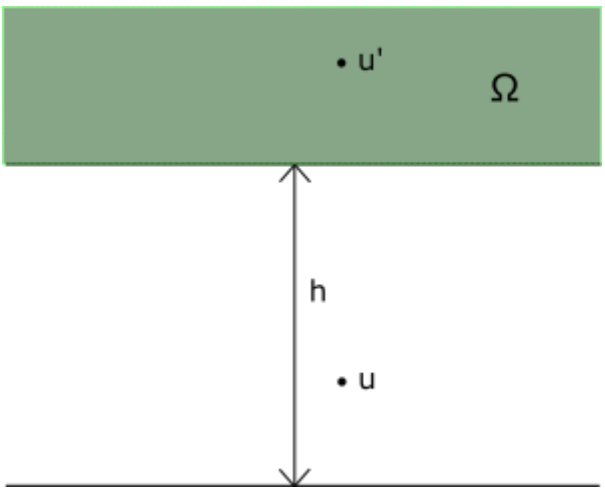

Figure 12: *The Poincaré half-plane with the origin cusp region Ω in green, Euclidean distance h and the point u before and after the shift.*

We can use this topology to learn more about the global structure of the cut locus. If a certain property would result in a different topology, like extra boundaries, that property can not hold. Cusps and boundaries are all types of boundaries and if they are not connected to the cut locus there would be more than one boundary, which is a contradiction with the topology of the disk and so all of them must be connected to the cut locus. Multiple cut locus edges that end in a boundary is seen as one point, so these edges are connected and there are no loops around the boundaries. If the cut locus was not fully connected $H \setminus (\Sigma, \mathbf{C})$ would have two or more boundaries, this means the cut locus has to be fully connected. Lastly if there was a loop in the cut locus there would be an area disconnected from the rest of the surface, which is a contradiction with the topology of the disk and so there can not be any loops.

This means that at least one cut locus ends at each cusp or boundary, Σ is fully connected and Σ has no loops.

So, we can conclude that the cut locus is a single planar tree, which fully proves lemma 1. Lemma 1 shows that there are graphs associated to each hyperbolic surface, but the question is if there is a way to fully recover the hyperbolic surfaces from just the cut locus graphs? And more importantly do we even need to describe the full moduli space to find the Weil-Petersson volumes?

4 Defining the subspace $\hat{\mathcal{M}}_{g=0,n+1}$

Because the Weil–Petersson volume is an integral of a $(2n-4)$ form over the $(2n-4)$ dimensional moduli space [16], removing lower dimensional sub-manifolds does not change the Weil–Petersson volume. This is why we want to find a subspace $\hat{\mathcal{M}}_{g=0,n+1}$ that has the same dimension as $\mathcal{M}_{g=0,n+1}$, because it would have the same Weil-Petersson volume, but it could be much easier to work with. Multiple hyperbolic surfaces can have the same cut locus, but not all cut locus graphs have to contribute to the Weil-Petersson volume, so lets take a deeper look at these cut locus graphs and what surfaces they represent. Let Λ be the collection of possible cut locus graphs of $\mathcal{M}_{g=0,n+1}$. Before we said that all cut locus edges that pass a boundary meet in the boundary, but now that we want to describe these regions more completely we need to differentiate two situations here as they behave differently. If two cut locus edges intersect somewhere on the hyperbolic cylinder we say they meet in an internal vertex $v_i \in \mathbf{V}$, but if they never meet on the hyperbolic cylinder we say they meet at the boundary. These two situations can be seen in Figure 13. When we say a boundary of degree k we mean that k cut locus edges never meet each other on the hyperbolic cylinder and thus meet at the boundary. Having defined Λ the question becomes: Which cut locus graphs $\lambda \in \Lambda$ contribute to the Weil-Petersson volume? This is where lemma 2 comes in.

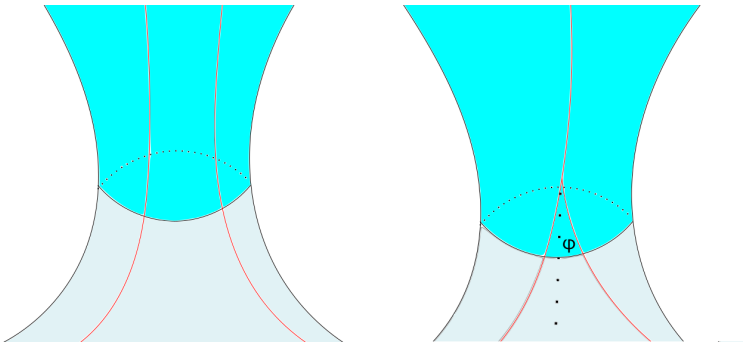

Figure 13: *Two cut locus edges that cross a hyperbolic cylinder. On the left they never converge while on the right they meet at some point. The angle φ between the cut locus and the shortest geodesic (that does not cross these cut locus edges) to the origin is shown where the cut locus edges meet. The dotted line is the geodesic that defines the φ coordinates.*

Lemma 2. *Let $\hat{\Lambda}$ be the collection of cut locus graphs of $\mathcal{M}_{g=0,n+1}$ where the tree has vertices of degree 3, except where the cut locus meets a boundary*[4]*. On these boundaries an arbitrary number of geodesic segments can meet, unless the boundary is a cusp, in which case only one line can meet there, this corresponds to a leaf of the graph. For the function $f : \mathcal{M}_{g=0,n+1} \to \Lambda$ that assigns a cut locus tree with coordinates to each hyperbolic surface, let $\hat{\mathcal{M}}_{g=0,n+1} \subset \mathcal{M}_{g=0,n+1}$ be the preimage of $\hat{\Lambda}$. Then the Weil–Petersson volumes of $\hat{\mathcal{M}}_{g=0,n+1}$ and $\mathcal{M}_{g=0,n+1}$ are equal.*

To prove this lemma we first need coordinates that can be defined for each hyperbolic surface in the moduli space, which distinguish the surfaces and that fully determine them. With these coordinates we can then show the dimension of sub-spaces of $\mathcal{M}$ and remove lower dimensional ones without changing the Weil-Petersson volume.

First we divide the surface into hyperbolic polygons. To do this we need to notice that by taking the union of the two shortest geodesics from the origin to $u \in \Sigma \setminus \mathbf{V}$ each cut locus geodesic arc defines a geodesic that goes from the origin, in-between two boundary components before returning to the origin. This means that for each set of two cut locus arcs there are two unique disjoint homotopy classes. Two disjoint curves in different homotopy classes have two unique disjoint geodesics in their respective homotopy classes, as shown in definition 2.1 in [19], which means that there is a unique shortest disjoint geodesic for each cut locus edge. Additionally these unique geodesics always intersect with their corresponding cut locus edge at a right angle. To show this you can project any cut locus segments with the corresponding horocycles onto the disk like in Figure 15. In this projection it is clear that the shortest geodesic meets the cut locus at a right angle. These unique geodesic divide the hyperbolic surface in ideal geodesic "polygons", where some of the "polygons have boundaries or cusps partly or wholly on the interior of the polygon. This means that not all polygons are true hyperbolic polygons. Each of these polygons have either a $v \in \mathbf{V}$,

[4] $\hat{\Lambda}$ is also decorated with a set of coordinates, but this decoration will be defined later.

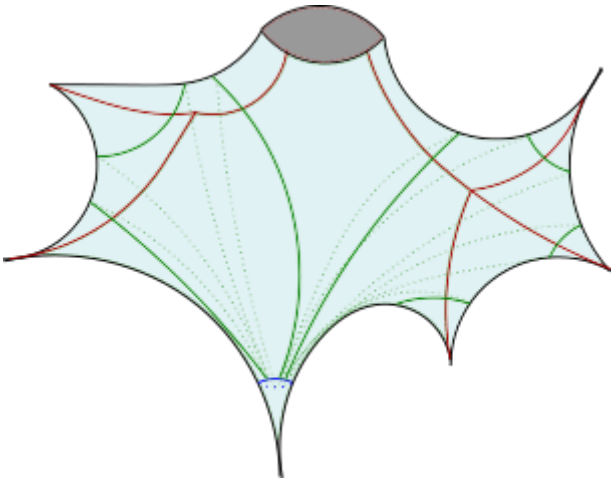

Figure 14: *A hyperbolic surface with the origin, 5 cusps and a boundary. The cut locus is shown in red. The green lines are the unique geodesics of each cut locus edge. The blue line is the horocycle of the origin. Dotted lines are on the back of the surface.*

a boundary component $\beta_i \in \mathbf{B}$ or a cusp $c \in \mathbf{C}$ corresponding to the polygon. An example of dividing a surface into these sections can be seen in Figure 14.

For each $v \in \mathbf{V}$ of degree k we define $\varphi_i \in (0, \pi)$ for $i = 1, ..., k$ as the angle between the i^{th} cut locus edge and the shortest geodesic to the origin that meets the vertex on the left hand side of the edge, as shown in Figure 16. These dotted geodesics, define triangles with the cut locus arcs. The cut locus intersects the boundaries, or can be extended uniquely to intersect the boundaries, of the polygon at a right angle and two edges that meet at a cusp converge meaning that angle is 0. This leaves just one angle undetermined to fully determines the hyperbolic triangle. The triangles with the φ_i, ρ_i are congruent because they share two sides and one angle is 0 for both triangles. This means that $\varphi_i = \rho_i$ and the total sum of angles $\sum_{i=1}^{k} \varphi_i + \sum_{i=1}^{k} \rho_i = 2\sum_{i=1}^{k} \varphi_i = 2\pi$. This gives a total of k angles, that add up to π, which means that you need $k - 1$ φ angles to describe the polygon corresponding to that vertex.

Each boundary of length L will be enclosed by k geodesics, or enclosing geodesics, where k is the number of incoming cut locus arcs. These enclosing geodesics form a sort of hyperbolic polygon like before, but now with a boundary on the interior. This difference in internal structure means it is not a real hyperbolic polygon, but it is analogous to one, as it has the same number of enclosing edges. This means that boundaries can be enclosed by just one or two geodesics. To fully characterise the region around the boundaries we need to know how the cut locus edges behave if the surface is extended by adding a hyperbolic cylinder on the boundary. If the cut locus edges intersect before infinity we just use the φ_i coordinates of before measuring the angles on the hyperbolic cylinder as can be seen in Figure 13. For the cut locus edges that do not meet before infinity we use a different type

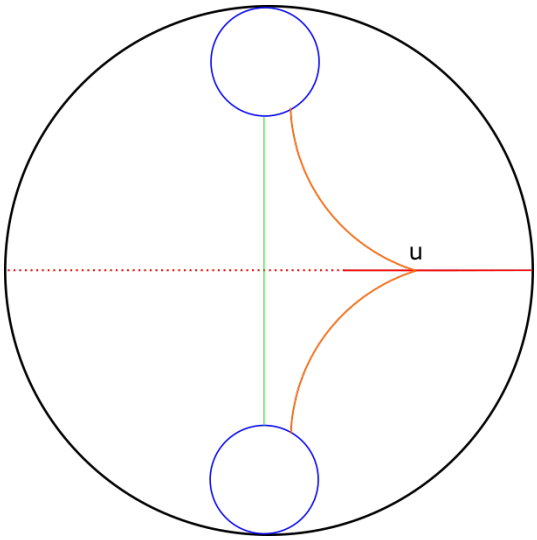

Figure 15: *The cut locus edge is the solid red line, which is extended into the dotted red line. The orange line is the union of the two shortest geodesics to the origin for a point u of the cut locus. The green line is then the unique shortest geodesic for that homotopy class.*

of triangulation.

If k cut locus edges reach infinity in the hyperbolic cylinder of a boundary, then there are k enclosing geodesics, which meet at the origin in k vertices. We subdivide this region into triangles by looking at geodesics that start from each vertex and then spiral into the boundary via the left hand-side, as shown in Figure 17. We will call these geodesics that spiral into the boundary spiraling geodesics. Two of these spiraling geodesics together with one enclosing geodesic then form a triangle that can be projected onto the hyperbolic half-plane, as shown in Figure 17. The distance x_i is the Euclidean distance in the projection between the start and end of the enclosing geodesics and q_i is the Euclidean distance in the projection from the right vertex of the enclosing geodesic to the end of the corresponding cut locus, as shown in Figure 17. These distances x_i, q_i exactly determine the area around the boundaries and we want to encode them in useful coordinates w_i, t_i. To define the w_i, t_i coordinates, we can combine the x_i, q_i in the equations

$$e^{w_i} = \frac{x_i + q_i}{q_i}, \tag{7}$$

$$e^{t_i} = \frac{q_i}{x_{i+1} + q_{i+1}}. \tag{8}$$

These coordinates are both ratios of the heights of geodesic arches. For w_i these are the two geodesic that meet the same cut locus in infinity, as shown in Figure 18. It turns out this ratio is also the hyperbolic distance between the cut locus segment and the geodesic that spirals into the boundary and meets the enclosing geodesic arcs at a right angle, as can be seen in Figure 17.

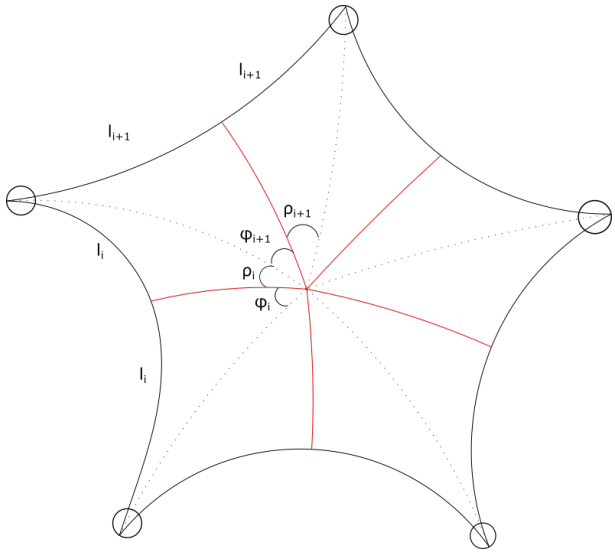

Figure 16: *A triangulation of a hyperbolic polygon. The cut locus is shown in red. The φ, ρ angles are the angles between the cut locus and the geodesic from the cusp that meets the central vertex. The circles are the horocycles of the origin and l_i is the hyperbolic distance between these horocycles as measured along the unique shortest geodesics of the homotopy classes.*

The t_i coordinates are a bit harder to showcase, but they are the ratio of the height of two geodesic arcs of geodesics that end in two neighboring cut locus edges, as shown in Figure 18. The two geodesics start at the same projection of the horocycle, but end at the two neighboring cut locus edges and the ratio of these geodesics are the t_i coordinates.

Because the k^{th} triangle is glued back to the first triangle there is a Möbius transformation with scaling factor e^L. This Möbius transformation also gives a restraint on the w, t coordinates: $\sum_i^k w_i = \sum_i^k t_i = \frac{L}{2}$ for each boundary.

The w_i, t_i coordinates exactly determine the height ratios of the geodesic arches shown in Figure 18. Section 5 will explain how to fully reconstruct and determine the area around the boundaries with the w_i, t_i coordinates.

When we want to describe the region around a cusp, the w_i coordinates will not work as they are positive $w_i > 0$ and $\sum w_i = \frac{L}{2}$, so the coordinates will all be zero when L goes to zero in the limit, which is the case for a cusp. Instead we will work with normalized coordinates $w_i' = \frac{2}{L} w_i$. These w_i' always sum up to 1 and are well defined even at $L = 0$. Any pair of geodesics that converge to a cusp also converge with each other and so all cut locus edges that meet a cusp end at the same point. This means that the t_i coordinates do not carry additional information and that the $\lim_{L \to 0} t_i = 0$. As a result a cusp where k cut locus edges meet has $k - 1$ independent w' coordinates and no independent t coordinates. With these coordinates we can fully describe any hyperbolic surface in $\mathcal{M}_{g=0,n+1}$.

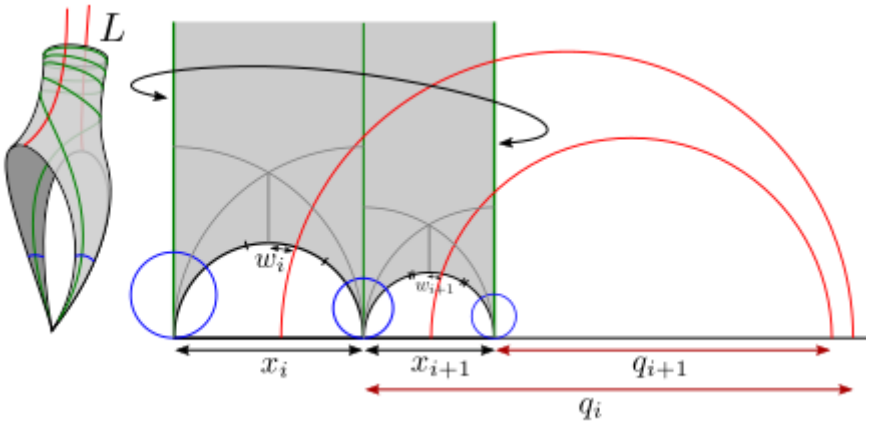

Figure 17: *On the left it shows a hyperbolic surface with a boundary component and two geodesic arcs that enclose it. The red lines are the cut locus geodesics, which are extended into infinity by adding a hyperbolic cylinder to the boundary. The green lines are the geodesics that spiral into the boundary from the origin. On the right the same surface is projected onto the Poincaré half-plane.* x_i, q_i *are the Euclidean distances between the arrows. The dotted lines are the geodesics from origin that meet the spiraling geodesics at a right angle.* w_i *is the hyperbolic distance between the arrows, as shown in the Figure.*

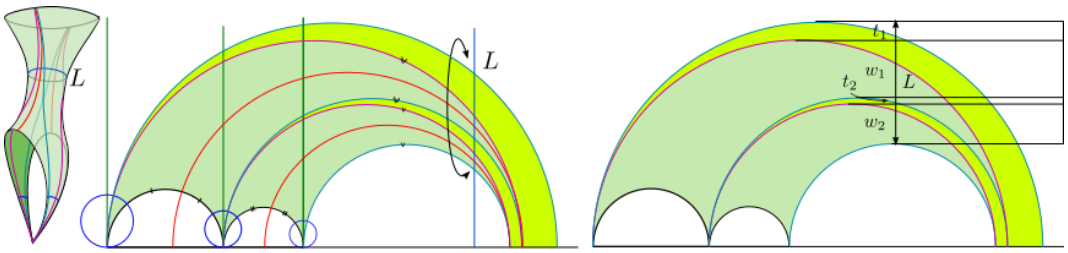

Figure 18: *The same projection of Figure 17 with additional geodesics from the cusp that converge to the cut locus edges at infinity. On the right the cut locus edges have been removed to show what distances the* w, t *coordinates are.*

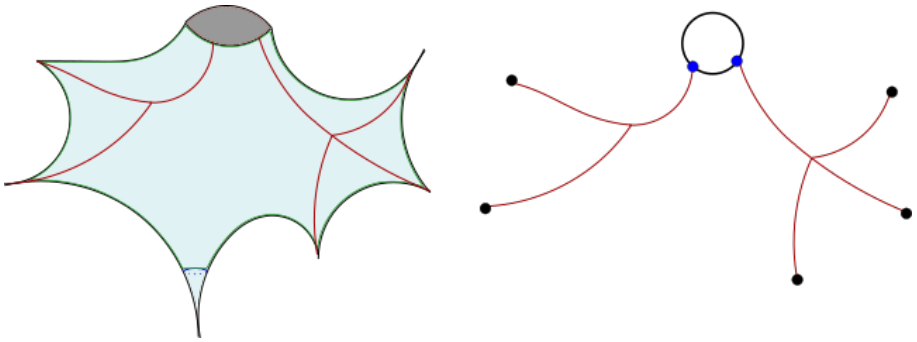

Figure 19: *A hyperbolic surface with its corresponding cut locus graph. The black dots represent the cusp vertices and the blue dots represent the boundary vertices. Lastly the black lines are the geodesic boundary segments between two boundary vertices and they count for the number of total edges in the graph.*

With these coordinates we can measure the dimension of different tree graphs. Remember that the moduli space is $(2n-4)$ dimensional and only spaces of that dimension will contribute to the Weil-Petersson volume. If a cut-locus tree spans a space with a lower dimension, because it has less than $(2n-4)$ coordinates, it can be removed from Λ without changing the Weil–Petersson volume. Now we just need to prove that the trees described in Lemma 2 are the only cut loci which need $(2n-4)$ coordinates to be described.

For a 3-regular tree on a hyperbolic surface with n boundary components, where boundary component meets only one cut locus edge, we need $(2n-4)$ coordinates to describe that set of hyperbolic surfaces. This is because in this situation the cut locus will have n leaves and for three regular trees the number of vertices will always equal $n-2$. For each three vertex there are 2 independent coordinates meaning $B=(2n-4)$. Therefore we must prove that each valid cut locus $c' \notin \hat{\Lambda}$ spans a subspace with a dimension of less than $(2n-4)$.

The best way of capturing this is by counting the dimension of an arbitrary cut locus. Let D be the dimension of the cut locus graph. $\mathbf{V}$, $\mathbf{B}$ and $\mathbf{C}$ are still respectively the collection of internal vertices (not on any boundary), boundaries and cusps with their cardinality as the non-bold same letter. To turn the cut locus in a full graph we turn each segment of a boundary into edges of the graph and each make each cusp a vertex, as can be seen in 19. With this graph let k_i be the degree of a vertex, cusp or boundary reflecting the amount of cut locus lines that meet there. V_0 is the collection of all vertices of the cut locus graph including those on boundaries and cusps. E is the collection of edges of the cut locus including the edges between vertices of a boundary as seen in Figure 19. The Euler characteristic of a sphere with B boundaries is $\chi = 2-B$.

The following relations can be found by counting how each type of vertex contributes

to the number of total vertices and edges

$$D = \sum_{v\in V}(k_v - 1) + \sum_{b\in B} 2(k_b - 1) + \sum_{c\in C}(k_c - 1),$$
$$\chi = 2 - B = V_0 - E + F = V_0 - E + 1.$$

This gives

$$V_0 = E + 1 - B,$$
$$2E = \sum_{v\in V} k_v + 3\sum_{b\in B} k_b + \sum_{c\in C} k_c,$$
$$V_0 = \sum_{v\in V} 1 + \sum_{b\in B} k_b + \sum_{c\in C} 1.$$

We can then eliminate E and V_0 to determine that the sum over boundaries is

$$\sum_{b\in B} k_b = \sum_{v\in V}(2 - k_v) + \sum_{c\in C}(2 - k_c) - 2 + 2B.$$

This allows us to calculate the dimension

$$D = \sum_{v\in V}(3 - k_v) - 4 + 2B + \sum_{c\in C}(3 - k_c) \leq 2(C + B - 2) = (2n - 4), \tag{9}$$

which is maximal only when $k_v = 3$ and $k_c = 1$ $\forall v \in \mathbf{V}$ and $\forall c \in \mathbf{C}$. These trees have the maximal dimension of $(2n - 4)$. To illustrate why these graphs are described by more coordinates you can compare some sample graphs and their dimension as seen in Figure 20. Therefore $\hat{\Lambda}$ is the collection of cut loci that have the maximal dimension of a given moduli space $\mathcal{M}_{g=0,n+1}(\mathbf{L})$ and all other diagrams can be removed without changing the Weil-Petersson volume. This proves lemma 2.

This means that $\hat{\mathcal{M}}_{g=0,n+1}$ and $\mathcal{M}_{g=0,n+1}$ have the same Weil-Petersson volumes. If we can completely describe $\hat{\mathcal{M}}_{g=0,n+1}$ with $\hat{\Lambda}$ we could use it to find the Weil-Petersson volumes. But for this strategy to work the two spaces need to be completely equivalent or in other words we need a bijection between the two.

5 Decorating $\hat{\Lambda}$ and bijection to $\hat{\mathcal{M}}_{g=0,n+1}$

To find a bijection, we need to know how to recreate hyperbolic surfaces from a decorated graph. So far we have not made concrete what decoration there is on the graphs. Let's make that concrete by defining $\hat{\Lambda}(\mathbf{L})$, where $\mathbf{L} = (L_1, L_2, ..., L_n)$. The space consists of the collection of finite trees $\lambda \in \hat{\Lambda}$ and a decoration of coordinates for each vertex in λ. There are tree types of vertices in λ. It has C vertices of degree one, which are all decorated with the length $L = 0$. λ has B vertices of arbitrary degree k_b decorated with $(w_{bi})_{i=1}^{k_b} \in (0,\infty)^{k_b}, (t_{bi})_{i=1}^{k_b} \in [0,\infty)^{k_b}$. The degree of the boundary vertices is limited by

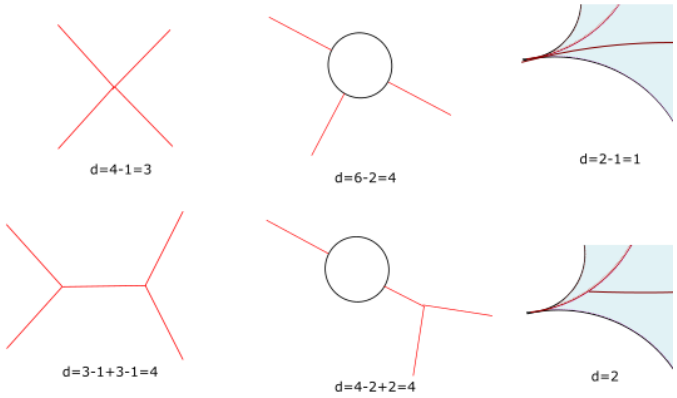

Figure 20: *Three different cut locus configurations (top) and their replacement (bottom) with the number of coordinates needed to describe the region for each situation. The cut locus graphs that meet a cusp on the right are shown on hyperbolic surfaces for clarity.*

the total dimension of the moduli space $2(n-2)$. If all coordinates are related to boundaries, each boundary of degree k_b will contribute $2(k_b-1)$ coordinates. Which means that $\sum_{b=1}^{B} k_b \leq C+2B-2$. Additionally two restrictions hold here for w,t: $\sum_{i}^{k} w_{bi} = \sum_{i}^{k} t_{bi} = \frac{L_b}{2}$.

Lastly $\mathbf{A}$ is the collection of internal vertices of degree 3 in λ. The number of these vertices is $A = (n-2) - \sum_{b=1}^{B}(k_b-1)$. These are decorated with the same $\varphi \in (0,\pi)$ coordinates as before. As there are now three angles for each vertex we will call them φ, χ and ξ, labeled counter clockwise. Each of these angles correspond to one cut locus edge and each edge is attached to either two inner vertices, two boundaries or a boundary and a vertex. This gives each edge two φ angles, one of which is zero in the case of a boundary. These φ angles have 2 restrictions. First around a vertex they must add up to $\varphi+\chi+\xi = \pi$. Secondly the two φ coordinates φ_i, φ_{i+1} of a cut locus edge are part of the same triangle, as can be seen in Figure 21, which means that $\varphi_i + \varphi_{i+1} < \pi$. This restriction is called the Delaunay condition. The first restriction means we only need the φ and χ coordinates for each boundary to fully determine the local structure, as long as $\varphi+\chi < \pi$ holds, this ensures $\xi < \pi$. We will call the collection of w, t, φ, χ coordinates that satisfy these restraints local coordinates. This decoration of the tree graphs fully defines $\hat{\Lambda}(\mathbf{L})$. With this subspace in mind we can try to find a bijection between it and the moduli subspace that produces it.

Theorem 3 (Bijection Theorem)**.** *Let $f : \hat{\mathcal{M}}_{g=0,n+1}(\boldsymbol{L}) \to \hat{\Lambda}(\boldsymbol{L})$ be the function that associates to $H \in \hat{\mathcal{M}}_{g=0,n+1}(\boldsymbol{L})$ the graph that is of the form of the cut locus of H and as the decoration the set of coordinates as measured on the surface H. Then f is a bijection.*

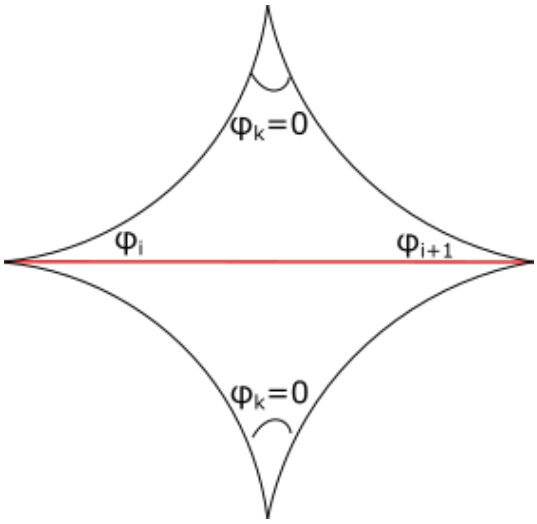

Figure 21: *The two identical triangles that the angles φ_i and φ_{i+1} coordinates define.*

Proof. The function f associates one cut locus graph and decoration to each hyperbolic surface. To prove that it is a bijection, we just need to prove that for $\forall \lambda \in \hat{\Lambda}$ $f^{-1}(\lambda)$ has exactly 1 preimage, or in other words a unique inverse. To start we need to define f^{-1}.

Let $\lambda \in \hat{\Lambda}$ be a decorated cut locus graph. To define the inverse $f^{-1}(\lambda)$ we generate a number of triangles and gluing relations to reconstruct a hyperbolic surface. Each edge of the cut locus has two φ_i coordinates, if a cut locus edge meets a boundary or cusp we define the corresponding angle $\varphi_i = 0$. We associate two identical triangles with angles $\varphi_1, \varphi_2, 0$ to each edge, as shown in Figure 23. Because at least two of the edges of the triangle end at a vertex there is no ambiguity when gluing these triangles together. The triangles are glued together to their identical partner and other triangles whose cut locus edges share a vertex. The triangles associated to cusps are glued together with two edges instead of one as can be seen with the arrows in Figure 23. This procedure works for all edges of the cut locus, but there is still an area around the boundaries which is not specified.

For the area around a boundary we have $(w_i, t_i)_{i=1}^k$ where $\sum_i w_i = \sum_i t_i = \frac{L}{2}$. To construct the hyperbolic triangles, we start by looking at the Poincaré half-plane and defining a geodesic arc starting at $z = -1$ and ending at $z = 1$. We then construct additional geodesic arcs iteratively. The radius of the arc is e^{w_i} or e^{t_i} times larger than the previous one and starts at one of the end points of the previous arc, as shown in Figure 22. So, the radii of the first 4 arcs are respectively $1, e^{w_1}, e^{w_1+t_1}, e^{w_1+t_1+w_2}$ and one of its end points is the end of the previous arc. For example the second arc is of radius $1 \cdot e^{w_1}$ and starts at $z = 1$. The

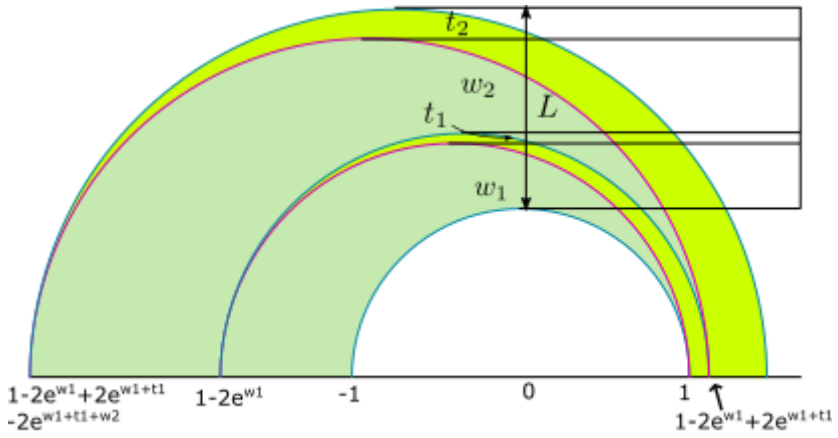

Figure 22: *The reconstruction of the geodesic arcs in the upper half-plane.*

coordinates where the arcs intersect the real axes are encoded in the iterative function

$$\gamma_0 = 1, \tag{10}$$

$$\gamma_n = \gamma_{n-1} + 2\prod^{\frac{n}{2}} e^{w_i} \prod^{\frac{n}{2}} e^{t_i} \text{ For n=even}, \tag{11}$$

$$= \gamma_{n-1} - 2\prod^{\frac{n+1}{2}} e^{w_i} \prod^{\frac{n-1}{2}} e^{t_i} \text{ For n=odd}. \tag{12}$$

The last geodesic arc end points are then $(\gamma_{2k-1}, \gamma_{2k})$. The first and last arcs are glued together in our reconstruction, so there must be a Möbius transformation g connecting the two, which also reproduces the boundary length L and it keeps ∞ fixed. The Möbius transformation $g(z) = az + b$ can send the first arc coordinates (-1,1) to the last arcs coordinates and keeps ∞ fixed. To do this $a = e^{\sum^k w_i} e^{\sum^k t_i} = e^L$ and $b = \gamma_{2k-1} + e^L$. This means that g just re-scales the hyperbolic height by L, in addition to a constant shift on the real axis equal to b. Therefore these arcs define triangles around a boundary of length L.

By defining these arcs we can reproduce Figure 17 and thus reconstruct the area around the boundaries. This combined with the previous ideal triangles defines a hyperbolic surface for each cut locus graph $\lambda \in \hat{\Lambda}$ and so defines $f^{-1}(\lambda) = h'$. An example of the triangles this creates and how they are glued together are shown in Figure 23. With this definition of the inverse we just need to prove that $\forall \lambda \in \hat{\Lambda}, \forall h \in \hat{\mathcal{M}}$, $f(f^{-1}(\lambda)) = \lambda$ and $f^{-1}(f(h)) = h$ to prove theorem 3.

To start the proof let $\lambda' = f(h)$. $f^{-1}(\lambda')$ is then made up of triangles with angles φ_i, which are the same as h per construction. Around the boundaries the ratios that define w, t are also the same and so the same hyperbolic surface is constructed and $f^{-1}(f(h)) = h$.

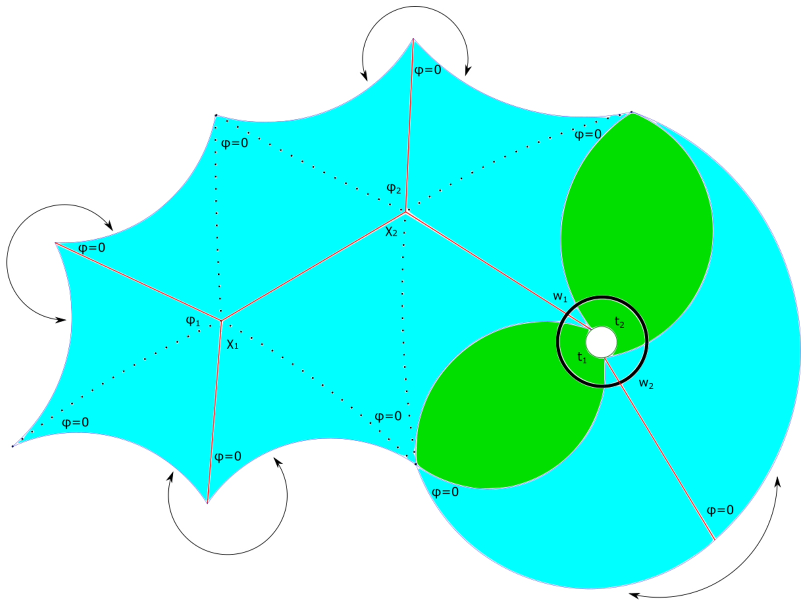

Figure 23: *The reconstruction of a hyperbolic surface from a decorated cut locus with two inner vertices and a boundary. The blue part of the surface is defined by the φ coordinates while the green part is constructed with the w, t coordinates. The arrows show which sides of the triangles are glued together.*

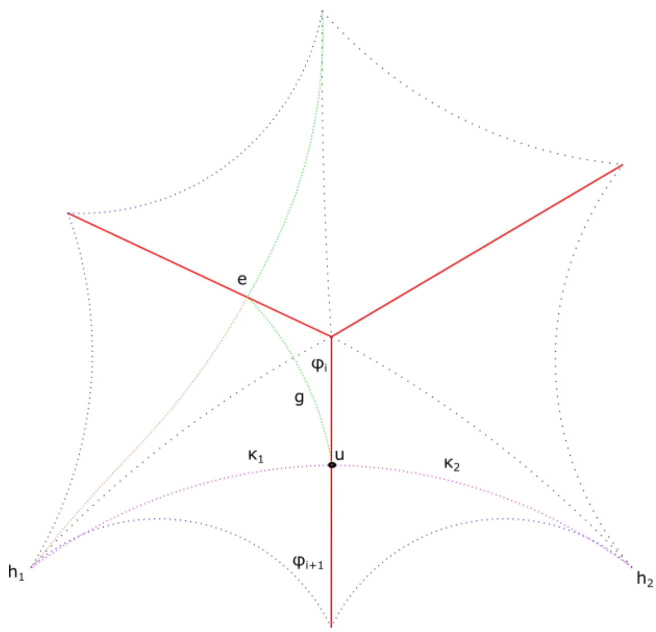

Figure 24: *A point u on the cut locus, with the two shortest paths κ_1, κ_2 to two projections of the origin h_1, h_2 in purple. The green lines form a hypothetical other shortest path g, which crosses the cut locus at point e. This path splits in two because the cut locus always has at least two shortest paths and this additional path is shown in orange.*

To check that $f(f^{-1}(\lambda)) = \lambda$, let $h' = f^{-1}(\lambda)$. We need to prove that λ is the cut locus of the hyperbolic surface h'. Take a point $u \in h'$ that lies on one of the edges of the cut locus λ, as shown in Figure 24. These points have two identical triangles attached to them, which means there are at least two geodesics κ_i to the origin or at least three of them if the point is a vertex of λ. Let us assume there is a shorter or equally short path g, shown in green in Figure 24. The part of the hyperbolic surface that can be reached without crossing the cut locus has two to three projections h_i of the origin, which all have a unique shortest path κ_i associated to them already. For g to be another geodesic to the origin it must therefore cross the cut locus somewhere else than in u. This crossing point e has at least two geodesics of equal length to the origin and one of these geodesics will go to one of the projections of the origin h_i. Path g is then of equal length as two sides of a triangle combined. The other side of this triangle is a κ_i and due to the triangle inequality g can not be as short or shorter than that κ_i. Therefore the point u has only the original two to three shortest paths κ_i to the origin and no more. Points not on λ have one shortest path with the same argument. This means that the cut locus of h' is λ and the angles are the same due to the construction $f(f^{-1}(\lambda)) = \lambda$. Therefore f is a bijection which proves theorem 3.

This implies that we can do any calculation for the Weil-Petersson measure in the corresponding space of decorated trees, as the two spaces are equivalent. Additionally this connection can be used to further investigate other properties of moduli spaces, by studying the corresponding trees. We can now try to calculate the Weil-Petersson measure using this space of trees $\hat{\Lambda}$. With that measure we encode the contribution to the JT path integral of each part of a moduli space.

6 Linking the Weil–Petersson measure to the Poison algebra

We can uniquely describe all of the hyperbolic surfaces in the moduli space using the tree bijection. But we still need to now the Weil-Petersson measure, to know the contribution of each hyperbolic surface to the Weil-Petersson volume.

If we determine the coordinate basis of a tree $\lambda \in \hat{\Lambda}(\mathbf{L})$, we can calculate the corresponding Weil-Petersson measures via the Weil-Petersson Bracket.

The Weil-Petersson bracket is a Bivector, that corresponds to the Poison algebra of the coordinates of the surface. We will simply call the Weil-Petersson bracket the Poison algebra from now on. In general the Poison algebra will depend on the set of coordinates of the surface and the Poison product assigns $\{x_i, x_j\} = M_{ij}$ to each couple of coordinates x_i, x_j. The Poison algebra is antisymmetric meaning $M_{ij} = -M_{ji}$.

The Weil-Petersson measure μ_{WP} is the product of the Weil-Petersson form ω. ω in a general set of coordinates x_i is defined by

$$\omega = \sum_{ij} a_{ij} dx^i \wedge dx^j, \tag{13}$$

where $1 \leq i, j \leq 2m = 2(n-2)$ as $2m$ is the number of independent coordinates of the moduli space. The Weil-Petersson measure is then simply the product of ω

$$\begin{aligned}\mu_{WP} &= (2\omega)^m, \\ &= 2^m \omega \wedge \omega \cdots \wedge \omega, \\ &= 2^m \mathrm{Pf}(2a) dx^1 \wedge \cdots dx^{2m}, \\ &= 2^{2m} \sqrt{\det(a)} dx^1 \wedge \cdots dx^{2m},\end{aligned}$$

where the blue extra factor of 2 in the Weil-Petersson measure μ_{WP} is there because of a difference in convention between the standard Kahler 2-form in Equation 25 we start with later and the Weil-Petersson measure used to calculate Weil-Petersson volumes. You can see this difference in equation 2.8 from [20] and Theorem 3.3.6 from [21].

The Poison algebra is then related to the inverse of the Weil-Petersson measure ω by the equation

$$\{x_i, \omega\} = dx^i = \sum_k M_{ik} \frac{\partial}{\partial x_k} \omega = \sum_k M_{ik}(a_{kj} dx^j - a_{lk} dx^l). \tag{14}$$

From this equation we can relate the indices of M_{ij} and a_{ij} by

$$\delta_{ij} = \sum_k 2 M_{ki} a_{kj}, \tag{15}$$

$$M_{ij} = \frac{1}{2} a_{ij}^{-1} = \{x_i, x_j\}, \tag{16}$$

such that the determinants are related by

$$\sqrt{\det(a)} = 2^{-m} \frac{1}{\sqrt{\det(M)}}. \tag{17}$$

If we put these relations together we can find the Weil-Petersson measure by just calculating the determinant of the Poison algebra[5]

$$\mu_{WP} = \frac{2^m}{\sqrt{\det(M)}} dx^1 \wedge dx^2 \wedge \cdots dx^{2m}. \tag{18}$$

The Poison algebra related to the Kahler two form is already known for hyperbolic surfaces in another set of coordinates; the shear coordinates [19]. The only problem is that this Poison algebra is not in the coordinates we have used for the bijection, which means we need to find the link between the local coordinates and the shear coordinates. To understand the link between these coordinates we must first know what shear coordinates are.

[5] We drop the $\frac{1}{(n-2)!}$ factor as it is not important in the calculations within this thesis. It can be safely ignored as it is just an overall factor when you actually calculate Weil-Petersson volumes.

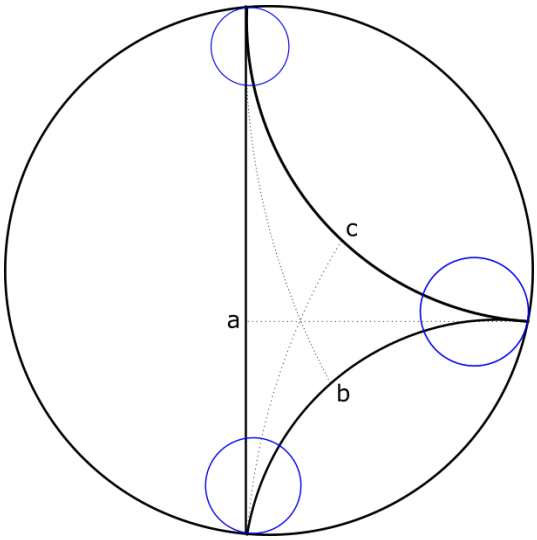

Figure 25: *An ideal triangle in the Poincaré disk. Horocycles are shown in blue. The dotted lines are the geodesics that meet the opposing sides at a right angle defining the unique points a, b, c.*

6.1 Shear Coordinates

There is a ambiguity when gluing infinitely long sides of triangles together. When you try to glue two infinitely long sides together, there is always the freedom to shift the two sides relative to each other before gluing them together. This ambiguity needs to be resolved to fully determine the hyperbolic surface. If we could mark unique points on all sides of the triangles, we could then measure the distance between these points to fully determine this shift. These hyperbolic distances is what we call the shear coordinates.

To define the shear coordinates we look at the geodesic of the opposing vertex that meets the side at a right angle, as shown in Figure 25, for each ideal triangle side. Because geodesics are half circles in the Poincaré half-plane there is a unique one that meets the side at a right angle, as shown in Figure 26, which defines these marked points uniquely. Each time we want to glue two sides together we will have two unique marked points. We then measure the hyperbolic distance from left to right on the side of the triangle. This distance is the shear coordinate for that edge.

The ideal triangulation we made in Section 4 associates one side of an ideal triangle to each cut locus edge of the cut locust tree on our hyperbolic surface. Therefore we get one shear coordinate for each cut locus edge in the cut locus $\lambda \in \hat{\Lambda}$. To find the basis of the shear coordinates we need to know the restrictions on them. There is a Möbius transformation which restricts the shear coordinates for the origin and each boundary. This results in $\sum_{k=1}^{K} z_k = 0$ and $\sum_{i=1}^{k_b} z_i = L$ where K is the collection of all shear coordinates and

k_b is the sum of edges around the face of a boundary.

Sometimes it is easier to measure the distances within the triangle and later add them together to get the shear coordinates. That is why we measure the distance r from where the cut locus meets the edge that it defines[6] and the marked point from left to right. This distance r can be measured for each triangle and there are two r coordinates for each edge, which add up to the corresponding z coordinate as can be seen in Figure 26. With all this in mind we can start looking at the connection between the coordinates.

6.2 Internal vertex angles

As mentioned before we have three angles φ, χ, ξ counter clockwise around an internal vertex. The question is how these coordinates are related to the shear coordinates. To relate the φ coordinates to the shear coordinates we need an in between step. Because the r coordinates can immediately be linked to the angles between two cut locus edges in a vertex $v \in \mathbf{V}$ we can use them to find the connection to the shear coordinates. We can simply relate the φ coordinates to the angles between to cut locus edges by $\alpha = \pi - \varphi$, $\beta = \pi - \chi$ and $\gamma = \pi - \xi$, as they are linear combinations of these angles, which can be seen in the left side of Figure 28. From these definitions we know that $\sin(\alpha) = \sin(\pi - \varphi) = \sin(\varphi)$.

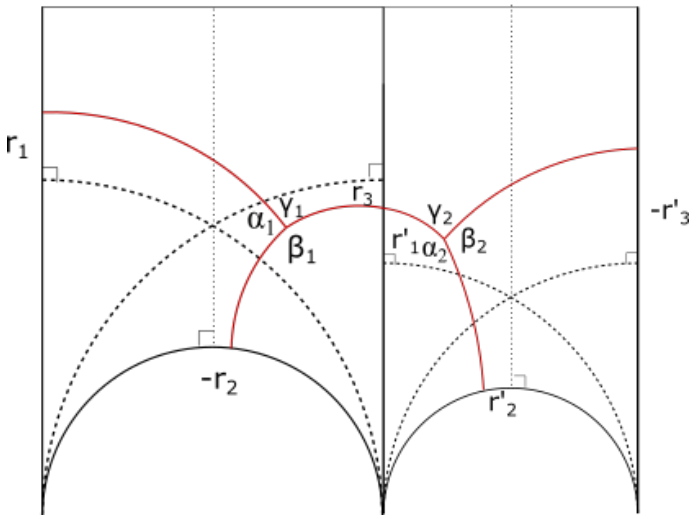

Figure 26: *Two ideal hyperbolic triangles drawn in the Poincaré half-plane projection. In red the cut locus is drawn with the corresponding angles α, β, γ. The dotted lines are geodesics that go from one of the vertices of the triangle, which meets the opposing side at a right angle. These uniquely define points on each side of the triangle. The distances r are the hyperbolic distances between the cut locus and these unique points. The sum of the r coordinates form the z coordinates, so $r_3 + r'_1 = z_1$ in the Figure.*

[6] If the cut locus edge does not meet the edge it can be uniquely extended, so that it does.

Because these angles only determine the interior structure of each triangle, we can only relate them to the distance r between the marked point and the cut locus edge, as shown in Figure 26. The sum of these hyperbolic distances is then the shear coordinate. These angles are related to the hyperbolic distances r by the hyperbolic law of sines

$$e^{r_1} = \frac{\sin(\alpha)}{\sin(\gamma)} = \frac{\sin(\varphi)}{\sin(\xi)} = \frac{\sin(\varphi)}{\sin(2\pi - \varphi - \chi)}, \tag{19}$$

$$e^{r_2} = \frac{\sin(\beta)}{\sin(\alpha)} = \frac{\sin(\varphi)}{\sin(\chi)}, \tag{20}$$

$$e^{r_3} = \frac{\sin(\gamma)}{\sin(\beta)} = \frac{\sin(\xi)}{\sin(\chi)} = \frac{\sin(2\pi - \varphi - \chi)}{\sin(\chi)}. \tag{21}$$

By multiplying these three formulas together you get an additional constraint: $r_1 + r_2 + r_3 = 0$, which corresponds to the restriction that $\varphi + \chi + \xi = \pi$. This means we can transform the φ, χ coordinates to the r coordinates and then determine the shear coordinates. This works for all the internal vertices, but we still need to link the w, t coordinates to the shear coordinates, to describe the full set of local coordinates.

6.3 The boundary coordinates w, t

The shear coordinates around the boundaries are simply related to the x_i distances by $e^{z_i} = \frac{x_i}{x_{i+1}}$. This is because the geodesic arcs that mark the unique point are half circles with radius x_i.

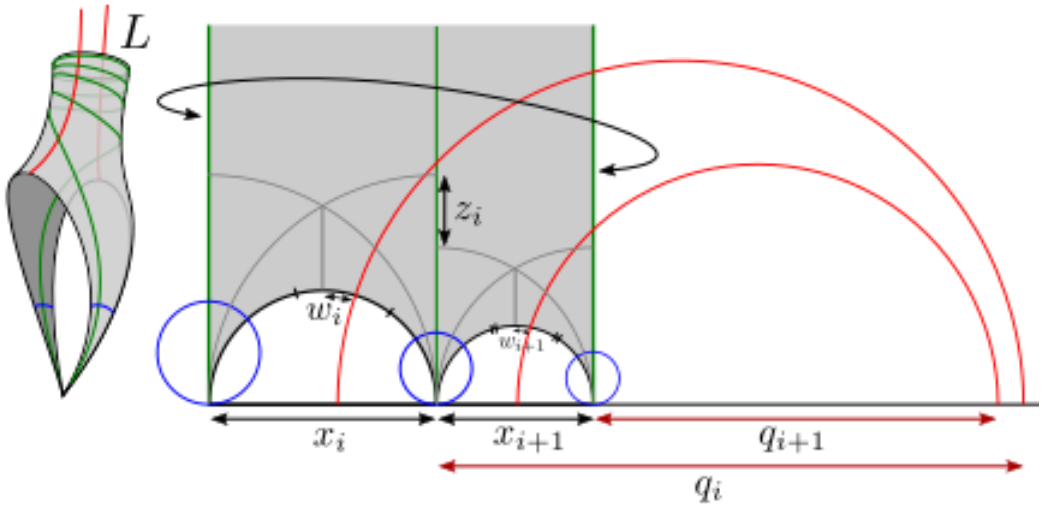

Figure 27: *The geodesic arcs that define the marked points and the corresponding shear coordinates.*

The w_i coordinates are just $-r_i$ coordinates, as shown in Figure 27, as it is exactly the opposite of the r coordinate definition.

The remaining shear coordinates can be linked to the w, t coordinates with some simple algebra resulting in

$$e^{z_i} = e^{t_i} \frac{e^{w_i} - 1}{1 - e^{-w_{i+1}}}, \tag{22}$$

$$z_i = t_i + \ln(e^{w_i} - 1) - \ln\big(1 - e^{-w_{i+1}}\big). \tag{23}$$

The Möbius transformation that identifies the first triangle side to the last gives rise to the constraint: $\sum_{i=1}^{k_b} z_i = L$.

Each shear coordinate can now be described by the local coordinates.

7 The local Poison algebra

Now that we know the relation between the shear and local coordinates we can try to transform the Poison algebra into the new coordinates. We can do this by making an Ansatz of the form of the Poison algebra and then checking that the two Poison products agree on the possible combinations of the basis coordinates. It turns out this is simplest to do if you check the Poison product of the shear coordinates.

We start with an Ansatz of the form of the local Poison algebra

$$\{\cdot\,,\cdot\}_{\text{local}} = \sum_{a=1}^{A} \frac{\partial}{\partial \varphi_a} \wedge \frac{\partial}{\partial \chi_a} + \sum_{b=1}^{B} \sum_{j=1}^{k_b} \frac{\partial}{\partial t_{j,b}} \wedge \left(\frac{\partial}{\partial w_{j,b}} - \frac{\partial}{\partial w_{j+1,b}} \right), \tag{24}$$

where a sums over all vertices not connected to a boundary, b sums over all boundaries and j sums over all w, t in each loop.

The Poison algebra in shear coordinates has the form [19]

$$\{\cdot\,,\cdot\}_{\text{shear}} = \sum_{v}^{V} \sum_{i=1}^{3} \frac{\partial}{\partial z_{v_i}} \wedge \frac{\partial}{\partial z_{v_{i+1}}}, \tag{25}$$

where V is the collection of vertices, including those connected to boundaries, and $z_{v_{i+1}}$ is defined counter clockwise to z_{v_i}.

The shear coordinates only depend on the local coordinates associated to their vertices. This ensures that if the edges of two shear coordinates z_i, z_j do not share a vertex the products $\{z_i, z_j\}_{\text{shear}} = \{z_i, z_j\}_{\text{local}} = 0$. Or inversely, both Poison algebras can only have non zero products if the two coordinates share a vertex. This means we just have to look at all combinations of shear coordinates around an internal vertex and around a boundary vertex.

For an internal vertex all shear coordinates are made up of two r contributions $z_i = r_i + r'_i$, $z_j = r_j + r'_j$. We labels the r coordinates so that r_i, r_j are dependent on the

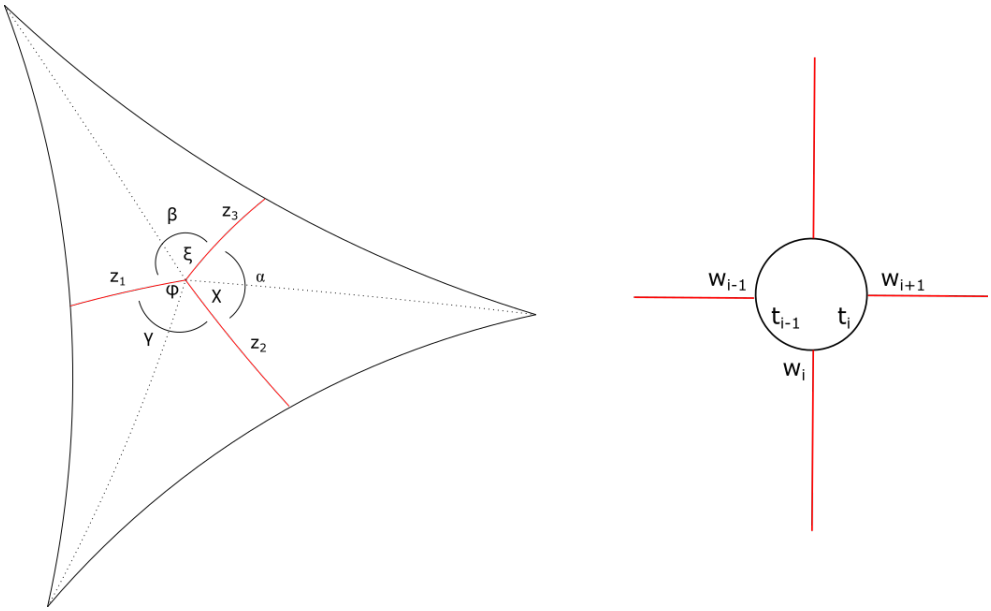

Figure 28: *The 6 types of z coordinates that need to be checked for the Poison algebra and their orientation with respect to one another. On the left is an internal vertex and on the right a boundary of degree 4. Both are decorated with the relevant local coordinates.*

same angles, while r'_i, r'_j do not share any common coordinates with each other and the r_i, r_j. Because the local Poison algebra is only unequal to zero if the contributions share coordinates of the same vertex we can ignore the r', as they do not contribute to the product.

To calculate the contributions, we will look at the shear coordinates surrounding a vertex with angles φ, χ, ξ. These shear coordinates, as seen in Figure 28, are

$$z_1 = \ln\left(\frac{\sin(\xi)}{\sin(\chi)}\right) + r'_1,$$
$$z_2 = \ln\left(\frac{\sin(\varphi)}{\sin(\xi)}\right) + r'_2,$$
$$z_3 = \ln\left(\frac{\sin(\chi)}{\sin(\varphi)}\right) + r'_3.$$

The Poison product in the shear coordinates is simple, as we will organise all the z such that they are ordered counter clockwise, which makes the resulting shear Poison product 1. Now we just have to check that all these combinations are also one in the local Poison

product. The three combinations to calculate around an internal vertex are then

$$\{z_1, z_2\}_{\text{local}} = \frac{\partial z_1}{\partial \varphi}\frac{\partial z_2}{\partial \chi} - \frac{\partial z_2}{\partial \varphi}\frac{\partial z_1}{\partial \chi} = -\cot(\xi)\cot(\xi) + (\cot(\varphi) + \cot(\xi))(\cot(\xi) + \cot(\chi)) = 1,$$
$$\{z_2, z_3\}_{\text{local}} = \frac{\partial z_2}{\partial \varphi}\frac{\partial z_3}{\partial \chi} - \frac{\partial z_3}{\partial \varphi}\frac{\partial z_2}{\partial \chi} = (\cot(\varphi) + \cot(\xi))\cot(\chi) + \cot(\varphi)\cot(\xi) = 1,$$
$$\{z_3, z_1\}_{\text{local}} = \frac{\partial z_3}{\partial \varphi}\frac{\partial z_1}{\partial \chi} - \frac{\partial z_1}{\partial \varphi}\frac{\partial z_3}{\partial \chi} = (-1)^2\cot(\varphi)(\cot(\xi) + \cot(\chi)) + \cot(\xi)\cot(\chi) = 1.$$

These combinations are also one because of a cotangent identity.

We can then look at the other type of vertex: the boundary vertex. None of these edges share common φ coordinates, so all these contributions can be ignored and will be marked by r'. The same is true for any w' of other loops, which will simply be included in r'. The three shear coordinates can be seen in Figure 28 and are

$$\begin{aligned} z_4 &= t_i + \ln(e^{w_i} - 1) - \ln\big(1 - e^{-w_{i+1}}\big), \\ z_5 &= t_{i-1} + \ln(e^{w_{i-1}} - 1) - \ln\big(1 - e^{-w_i}\big), \\ z_6 &= r'_6 - w_i. \end{aligned}$$

We order the edges counterclockwise again, so the shear Poison products are all 1. The local Poison algebra contributions are then

$$\begin{aligned} \{z_6, z_4\}_{\text{local}} &= \left(-\frac{\partial z_6}{\partial w_i} + \frac{\partial z_6}{\partial w_{i+1}}\right)\frac{\partial z_4}{\partial t_i} = (-1)^2 = 1, \\ \{z_5, z_6\}_{\text{local}} &= -\frac{\partial z_5}{\partial t_{i-1}}\left(\frac{\partial z_6}{\partial w_{i-1}} - \frac{\partial z_6}{\partial w_i}\right) = (-1)^2 = 1, \\ \{z_4, z_5\}_{\text{local}} &= \frac{\partial z_4}{\partial t_i}\left(\frac{\partial z_5}{\partial w_i} - \frac{\partial z_5}{\partial w_{i+1}}\right) - \frac{\partial z_5}{\partial t_{i-1}}\left(\frac{\partial z_4}{\partial w_{i-1}} - \frac{\partial z_4}{\partial w_i}\right) = \frac{e^{w_i}}{e^{w_i} - 1} - \frac{e^{-w_i}}{1 - e^{-w_i}}, \\ &= \frac{e^{-w_i} + e^{w_i} - 2}{e^{-w_i} + e^{w_i} - 2} = 1. \end{aligned}$$

These 6 combinations are equivalent in both Poison algebras. As mentioned before, both Poison algebras can only have non zero products if the two coordinates share a vertex and so these six combinations are the only non zero contributions. This means that the two Poison algebras agree on all combinations of shear coordinates and thus they are equivalent. In Section 6 we showed that the Weil-Petersson measure is simply related to the determinant of the Poison algebra. We can calculate the determinant by determining all Weil-Petersson brackets of each possible coordinate combinations of the basis to create a matrix and then calculate the determinant of that matrix.

7.1 The Poison algebra determinant

To determine the determinant of the Poison algebra we first need to construct it's matrix representation M. Each component of this matrix $M_{ij} = \{x_i, x_j\}$ is the Poison product of two independent coordinates. The number of independent coordinates that contribute to M for a general graph $\lambda \in \hat{\Lambda}(\mathbf{L})$ are

$$(\varphi_a, \chi_a)_{a=1}^{A}, \left((w_{j,b}, t_{j,b})_{j=1}^{k_b-1}\right)_{b=1}^{B}. \tag{26}$$

We order these coordinates in two steps: first all the angle coordinates $\varphi_1, \chi_1, \varphi_2, \chi_2 ...$, and then alternating the w, t coordinates $w_1, t_1 ... w_{k-1}, t_{k-1}$ for 1 boundary after another. From this we can create the matrix M that represents the Poison product of all the possible combination of basis coordinates, starting with the φ_i coordinates:

$$\begin{array}{c} \\ \varphi_1 \\ \chi_1 \\ \varphi_2 \\ \chi_2 \\ \varphi_3 \\ \chi_3 \\ ... \\ ... \end{array} \begin{array}{c} \begin{array}{cccccccc} \varphi_1 & \chi_1 & \varphi_2 & \chi_2 & \varphi_3 & \chi_3 & ... & ... \end{array} \\ \begin{pmatrix} 0 & -1 & 0 & 0 & 0 & 0 & 0 & 0 \\ 1 & 0 & 0 & 0 & 0 & 0 & 0 & 0 \\ 0 & 0 & 0 & -1 & 0 & 0 & 0 & 0 \\ 0 & 0 & 1 & 0 & 0 & 0 & 0 & 0 \\ 0 & 0 & 0 & 0 & 0 & -1 & 0 & 0 \\ 0 & 0 & 0 & 0 & 1 & 0 & 0 & 0 \\ 0 & 0 & 0 & 0 & 0 & 0 & b & b \\ 0 & 0 & 0 & 0 & 0 & 0 & b & b \end{pmatrix} \end{array}$$

where the $b's$ represent the other coordinate contributions to the matrix.

To calculate $\det(M)$ we use that the angles φ and the coordinates for each boundary are completely separate for the local Poison algebra. This means we can write $\det(M)$ as:

$$\begin{array}{c} \\ \varphi_1 \\ \chi_1 \\ \varphi_2 \\ \chi_2 \\ \varphi_3 \\ \chi_3 \\ ... \\ ... \end{array} \begin{array}{c} \begin{array}{cccccccc} \varphi_1 & \chi_1 & \varphi_2 & \chi_2 & \varphi_3 & \chi_3 & ... & ... \end{array} \\ \begin{vmatrix} 0 & -1 & 0 & 0 & 0 & 0 & 0 & 0 \\ 1 & 0 & 0 & 0 & 0 & 0 & 0 & 0 \\ 0 & 0 & 0 & -1 & 0 & 0 & 0 & 0 \\ 0 & 0 & 1 & 0 & 0 & 0 & 0 & 0 \\ 0 & 0 & 0 & 0 & 0 & -1 & 0 & 0 \\ 0 & 0 & 0 & 0 & 1 & 0 & 0 & 0 \\ 0 & 0 & 0 & 0 & 0 & 0 & b & b \\ 0 & 0 & 0 & 0 & 0 & 0 & b & b \end{vmatrix} \end{array}$$

for this example, H would be three. The $\det(M)$ is then simply $= 1 \begin{vmatrix} b & b \\ b & b \end{vmatrix}$, where the 2x2 matrix represents the rest of the determinant that encodes all the boundaries.

We then calculate the contribution of each boundary separately:

$$
\begin{array}{c|cccccccc}
 & w_1 & t_1 & w_2 & t_2 & w_3 & t_3 & ... & ... \\
w_1 & 0 & 1 & 0 & 0 & 0 & 0 & 0 & 0 \\
t_1 & -1 & 0 & 1 & 0 & 0 & 0 & 0 & 0 \\
w_2 & 0 & -1 & 0 & 1 & 0 & 0 & 0 & 0 \\
t_2 & 0 & 0 & -1 & 0 & 1 & 0 & 0 & 0 \\
w_3 & 0 & 0 & 0 & -1 & 0 & 1 & 0 & 0 \\
t_3 & 0 & 0 & 0 & 0 & -1 & 0 & 0 & 0 \\
... & 0 & 0 & 0 & 0 & 0 & 0 & b & b \\
... & 0 & 0 & 0 & 0 & 0 & 0 & b & b
\end{array}
$$

Here we only write down a boundary of degree 4 resulting in 3 w, t coordinates in the basis. The resulting determinant for one boundary of degree $k = 1$ is $\begin{vmatrix} b & b \\ b & b \end{vmatrix}$.

If we combine the contributions of the angles and each boundary the total determinant is $\det(M) = 1$. This means we can simply use Equation 18 to get the Weil–Petersson form

$$\mu_{WP} = 2^A \mathrm{d}\varphi_1 \mathrm{d}\chi_1 ... \mathrm{d}\varphi_A \mathrm{d}\chi_A \prod_{b=1}^{B} 2^{k_b - 1} \mathrm{d}w_1 \mathrm{d}t_1 .. \mathrm{d}w_{k-1} \mathrm{d}t_{k-1}. \tag{27}$$

This means we just get the Euclidean measure scaled by a 2 for each set of coordinates φ_i, χ_i or w_i, t_i. This is an incredibly simple result, that holds for all possible cut locus graphs $\lambda \in \hat{\Lambda}$. It makes further calculations much easier and is on itself a nice result.

We have derived two results that we can use as tools within JT gravity. We have a space of trees that is equivalent to the reduced moduli space and the Euclidean measure. To prove that we can use these tools in JT gravity we will derive the string equation that arises for moduli spaces with 2 marked cusps as we already know that it holds and what it's form is.

8 String Equation

To start deriving the string equation geometrically we need to know in what context it shows up. Let us look at the exponential generating function of WP volumes with two marked cusps and genus zero, which is

$$R = \sum_{n \geq 1} \frac{1}{n!} \int_0^\infty \prod_{i=1}^{n} \mathrm{d}q(L_i) V_{0,n+2}^{WP}(0, 0, L_1, L_2, ...). \tag{28}$$

Here $\mathrm{d}q(L_i) = q(L_i)\mathrm{d}L_i$ and $q(L_i)$ is an arbitrary density defined on the interval $[0, \infty)$, it takes the roll of the generating variable of the generating function. This is analogous to a source term $J(x)$ in QFT.

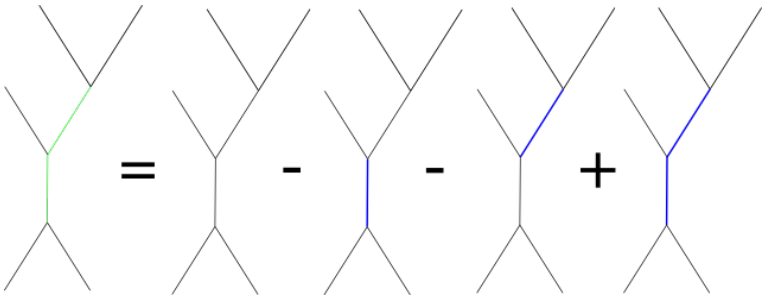

Figure 29: *The inclusion exclusion principle used on a binary tree with 5 leaves. The green edges are with the normal constraint $\varphi_i + \varphi_j < \pi$, black edges do not have this constraint and blue edges have the inverted constraint $\varphi_i + \varphi_j > \pi$.*

The Weil-Petersson volumes can be recovered from the generating function R by taking functional derivatives with respect to the boundary lengths. One functional derivative recovers

$$\frac{\delta R}{\delta q(L_1)}\bigg|_{q=0} = V_{0,3}^{WP}(0,0,L_1), \tag{29}$$

and for each additional functional derivative $\frac{\delta}{\delta q(L_i)}$ a boundary of length L_i is added to the Weil-Petersson volume.

The generating function R satisfies the string equation

$$R = \sum_{s=0}^{\infty} \frac{2^{s-1}}{s!}(t_s + \gamma_s)R^s, \tag{30}$$

$$\gamma_s = \frac{(-1)^s \pi^{2s-2}}{(s-1)!}\mathbf{1}_{s\geq 2}, \tag{31}$$

$$t_s = \frac{2}{s!}\int_0^{\infty} \left(\frac{L}{2}\right)^{2s} \mathrm{d}q(L). \tag{32}$$

Can this string equation be derived from the rooted trees? Using the Weil-Petersson measure we derived, R is simply the sum over all trees and the integral of the Euclidean measure of Equation 27 over their coordinates

$$R = \prod_{i=1}^{n} \int_0^{\infty} \mathrm{d}q(L_i) \sum_{\text{all trees } \lambda\in\Lambda} \int_{\text{coordinate ranges}} 2^A \mathrm{d}\varphi ... \prod_b 2^{k_b - 1} \mathrm{d}w \mathrm{d}t .... \tag{33}$$

To get the recursive formula seen in the string equation we need to split a general graph into a contribution we can calculate with s times a general graph attached, which will contribute the R^s. A boundary of degree $s+1$ is a great candidate for this, but what do we do with the internal graphs? To get a good candidate here we will use the inclusion exclusion principle on the collection of binary graphs with $s+1$ leaves.

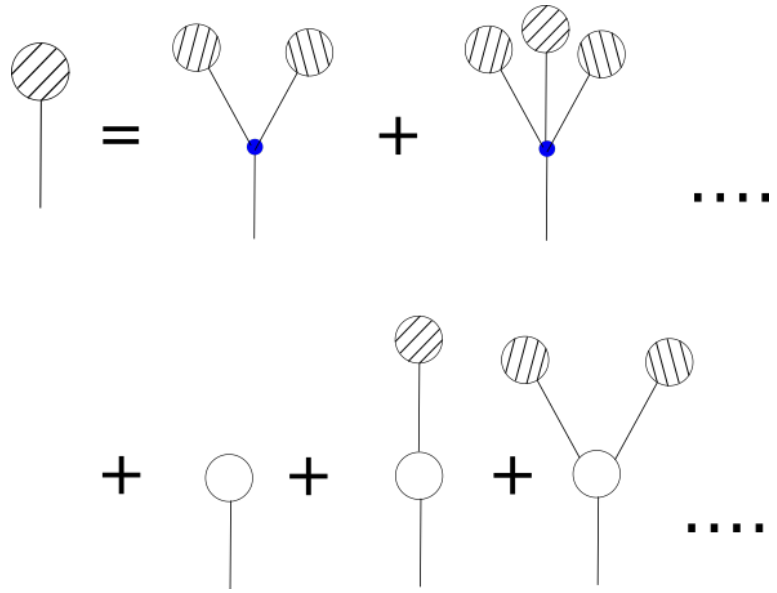

Figure 30: *On the left we have a general rooted cut locus graph. This rooted edge can first meet a boundary of degree $s+1$ with s times a general graph attached to it. Or the same story with a blue vertex of degree $s+1$ except this one only starts at degree 3.*

To see why this works let's look at a binary graph with our normal constraints $\varphi_i+\varphi_j < \pi$ for each edge of the graph. To get this same integral range we can lift the constrictions on all edges, which would over count the contributions and then use the inclusion exclusion principle, with the inverted condition $\varphi_i + \varphi_j > \pi$, to compensate for this. This means that for each edge with the inverted condition we get a factor of -1, as can be seen in Figure 29.

Then instead of using the inclusion exclusion principle on the collection of trees we can instead construct a new space of trees that sum up to the same contribution. Lets define a blue vertex of degree $s+1$, as all binary trees with the inverted constraint and a factor of $(-1)^s$. Then the space of trees with blue vertices and boundaries connected by edges without constraints gives the same space of trees that we started with. The generating function R can then be split into the contribution of a boundary of degree $s+1$ or a blue vertex of degree $s+1$, as can be seen in Figure 30. This means we just have to calculate the contribution of these vertices to find γ_s, t_s.

To do that we can look at the contribution of the collection of planar trees λ, with $s+1$ leaves and no boundaries. For each edge we know there is the inverted restraint: $\varphi_i + \varphi_j > \pi$. If we start with the φ_1 and χ_1 of a vertex of one of the leaves, for example the red and green angels in Figure 31, they add up to less than π. If we then look at the opposing angles, the orange and purple ones, as shown in Figure 31, we can use the inverted constraint to show these angles sum up to less than the green χ_1 and thus subdivide that green interval further. We can do this iteratively to mark $2s-2$ unique points e_i between $(0,\pi)$. Then each φ_i, χ_i subdivides the interval $(0,\pi)$ and we can integrate $2s-2$ of these

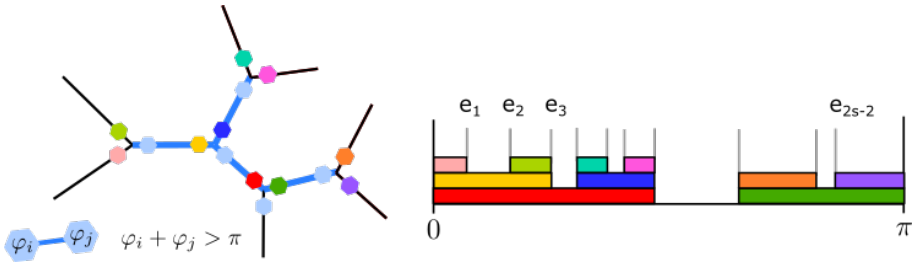

Figure 31: *A graph with inverted constraints. Each φ angle in the basis is given a color. Because of the inverted constraint, these angles subdivide the area $(0, \pi)$ into $2s-2$ parts marked with e_j.*

marked intervals with the condition: $\{e_1 < ... < e_{2s-2}\}$. We can then integrate over the full range $(0, \pi)$ and compensate for the over counting by dividing by $(2s-2)!$. The sum over planar trees is simply the Catalan numbers of binary trees with $s+1$ leaves. This contribution is shown in blue.

$$\begin{aligned}
&(-1)^s \sum_{\text{binary trees}} \int 2^{s-1} \mathrm{d}\varphi_1 .. \mathrm{d}\varphi_{2s-2}, \\
&= (-1)^s \mathrm{Cat}(s-1) \int_0^\pi 2^{s-1} \mathrm{d}e_1 .. \mathrm{d}e_{2s-2} \mathbf{1}_{\{e_1 < ... < e_{2s-2}\}}, \\
&= (-1)^s \mathrm{Cat}(s-1) 2^{s-1} \frac{\pi^{2s-2}}{(2s-2)!} = (-1)^s \frac{2^{s-1}\pi^{2s-2}}{s!(s-1)!} = \frac{2^{s-1}\gamma_s}{s!}.
\end{aligned}$$

We can use a similar trick to calculate the contribution of a boundary of degree $k = s+1$. This time let $e_j = \sum_{i=1}^{j} w_i$, the e coordinates now subdivide the interval $(0, L/2)$ in s steps, as $e_{s+1} = L/2$. This allows us to integrate over the full coordinate range, as long as we compensate for over counting by dividing by $s!$. The same trick is done for the t coordinates, which gives

$$\int_0^\infty \mathrm{d}q(L) \int_{\sum w_i = \sum t_i < \frac{L}{2}} 2^s \mathrm{d}w_1 \mathrm{d}t_1 ... \mathrm{d}w_s \mathrm{d}t_s = \int_0^\infty \mathrm{d}q(L) 2^s \frac{\left(\frac{L}{2}\right)^{2s}}{(s!)^2} = \frac{2^{s-1}}{s!} t_s.$$

These two factors combined exactly reproduce the string equation, this means the string equation can be derived geometrically, using the Weil-Petersson measure derived in Section 7.1. This gives us further inside into the connection between hyperbolic surfaces and algebraic derivations.

9 Results & Discussion

Previous approaches to finding the Weil-Petersson volumes used recursion formulas [13] to find them. These approaches only allowed us to calculate the Weil-Petersson volumes, but not the measures. In this thesis, we instead used a geometrical approach to derive the Weil-Petersson measure. Decorated cut locus graphs proved to be useful in describing the moduli spaces, especially after defining a subspace of equal Weil-Petersson volume, as there is a bijection between the two subspaces. This space of decorated tree graphs could then be combined with a newly derived local Poison algebra to derive that the Weil-Petersson measure is simply the Euclidean measure. With that measure the string equation could be derived by using graph recursion. With this small recap in mind, we can ask to what degree these results answer the research questions.

Can we describe the moduli space with decorated tree graphs? For each hyperbolic surface we can find a corresponding decorated tree. There is even a bijection $f : \hat{\mathcal{M}}_{g=0,n+1}(\mathbf{L}) \to \hat{\Lambda}(\mathbf{L})$. This means the subspace $\hat{\mathcal{M}}_{g=0,n+1}(\mathbf{L})$ can be fully described by decorated tree graphs, this allows us to more easily work with moduli spaces. It is however not yet clear if there is also a bijection for the full moduli space. The greatest and really only hurdle here is describing the area around a cusp, where multiple cut locus edges end, as it is not yet clear how the normalised w' coordinates recreate the area around the cusp. Because the subspace has the same Weil-Petersson volume this is not a problem for anything that only depends on the Weil-Petersson volumes or measure. The effect of cut locus graphs $\lambda \notin \hat{\Lambda}$ on problems that are not related to the Weil-Petersson volume would have to be investigated, as it is not clear that these would surfaces would have no contribution. The other limitation is that the proof in this thesis is only for genus 0, which means the tools can not yet be applied to situations with higher genus. All in all, the moduli spaces of genus 0 can almost completely be described by decorated tree graphs, except for a couple edge cases.

Is there a direct geometric way of evaluating the JT gravity path integral? The simple Weil-Petersson measure derived in this thesis describes a sort of density of states function for the moduli space. This can be used to reproduce Weil-Petersson volumes of moduli spaces with only isolated internal vertices, which agree with Mirzakhani's calculations [22]. There is however not a general formula for the Weil-Petersson volume with an arbitrary number of boundaries. To calculate this you would need to identify all possible cut locus trees and integrate over all the coordinates taking the Delaunay condition into account. The Weil-Petersson measure on it's own is already great evidence of this geometric approach working to evaluate the JT gravity path integral, as it can be used to calculate observables directly without first solving the full JT path integral, as I will elaborate on in the look forward. More importantly it gives a way to calculate observables within the JT path integral, which is a good extension of the model. The generating function of Weil-Petersson volumes could be a good way to evaluate arbitrary Weil-Petersson volumes, but

there is no known general form for this generating function. The string equation is the next best thing, as a solution to the string equation would be the generating function. Many of the properties of the generating function, such as it's asymptotic behavior when the number of boundaries goes to infinity, can be derived from the string Equation [23]. Although the string equation was already known from algebraic analysis the proof in this thesis gives an geometric derivation of it. It specifically gives a geometric interpretation of the two parts of the string equation t_s, γ_s. Here γ_s gets the interpretation of all cut locus graph with only internal vertices with $s+1$ leaves and the inverted Delaunay condition, while t_s gets the interpretation of a boundary with $s+1$ cut locus edges that meet the boundary and do not converge at some point on the hyperbolic cylinder. In short the derivation of the string equation is not its first derivation, but it is the first geometric derivation of it and this new derivation gives insights into the link between the string equation and parts of a hyperbolic surface.

Can decorated tree graphs and their Weil-Petersson measure be used to find a continuum limit of Moduli spaces? The continuum limit to the Brownian Sphere can be found by generating graphs and assigning distances within the graphs, before taking their continuum limit. We have found a unique way of generating tree graphs for a moduli space. The next step would be to find the distance statistics that govern distances on the cut locus graphs. These statistics are a type of observable for which the Weil-Petersson measure we derived could be used. It is however not yet clear how to exactly prove the form of the distance statistics, even though there are a few guesses what they would look like. Although we have not derived these statistics, when you are developing a new tool it is best to test it on something you already know the answer to. The better calibrated the new tool is the better it can be trusted when used on new problems, like the distance statistics. The String Equation was derived rather easily by combining the Weil-Petersson measure and the recursive nature of the cut locus graphs. This seems to shows that these two tools are well calibrated to the analysis of moduli spaces and it is a promising sign that it can give us the distance statistics that we need for a continuum limit of moduli spaces.

10 Conclusion and Look Forward

The graph description of Moduli spaces combined with the Weil-Petersson measure prove to be useful tools for further research within JT gravity. The simple local Poison algebra also indicates that the local coordinates could be useful in describing more complex systems.

With these tools in hand, what are the most promising avenues where these tools can be applied? To completely describe the moduli space the bijection in Section 5 could be continued to all of $\mathcal{M}_{g=0,n+1}(\mathbf{L})$. For this the inverse would need to be generalised for inner vertices of degree $k > 3$ and cusps with multiple cut locus edges. Describing the area around an inner vertex of degree $k > 3$ is easily continued using the φ_i coordinates. It is not clear however, how the area around a cusp with multiple cut locus edges could be described. This could maybe be solved by looking what the normalized w', t' coordinates do

under the $\lim_{L\to 0}$. Defining a local Poison algebra in this situation is also not immediately clear and more research would need to be done to determine the link to the larger set of φ coordinates and the shear coordinates. The inner vertices of even degree can not be related to the angles $\alpha, \beta, \gamma, ...$ between cut locus edges, as the system of equations degenerates. This means the approach used in this thesis will not work and a different link would have to be found.

For a higher genus the cut locus graphs would no longer be strictly tree graphs, but some form of graph with cycles in it. This would mean that the proof in Section 3 would have to be slightly altered to account for the new situation. The simple form of the local Poison algebra does however indicate that the local coordinates could be a good candidate for describing higher genus surfaces. The trick would be to understand what new restrictions would need to be added to the coordinates in this new situation to describe these higher genus surfaces. Additionally instead of having a marked cusp one could investigate hyperbolic surfaces without cusps and a marked boundary. Here the challenge would be to define something like a horocycle uniquely to measure distances to.

Next to describing moduli spaces exactly, the tree graphs can be used to understand the path integral better. Now that we have shown that the Weil-Petersson measure can be used to derive the string equation, the logical next step would be to start looking for new observables to calculate their correlation functions using this measure. A promising avenue is the calculation of distance statistics on hyperbolic surfaces and how these change within the moduli space. These distance statistics are so promising because for discrete surfaces a tree bijection exactly lead to distance statistics [9]. That is why a tree bijection is a promising avenue which could then be used to find the continuum limit to the Brownian sphere .

The simple form of the local Poison algebra also makes the local coordinates a good candidate to quantize. The local Poison structure is not more complicated than the standard poison structure in quantum mechanics. The Poison bracket $\{x, p\} = 1$ in classical mechanics and $\{\varphi, \chi\}_{\text{local}} = 1$ are the exact same form, while a similar form can be created with the w, t coordinates $\{t_i, w_j\}_{\text{local}} = \delta_{i,j} - \delta_{i,j+1}$. This gives a similar starting point, but quantizing the w and t coordinates will result in a new type of quantization. If these coordinates can be quantized it could allow for an interesting model to study quantized spaces within two dimensional gravity. In addition, combining hyperbolic surfaces could be possible owing to the simple coordinates, this could give a way of constructing higher-dimensional models.

In short the future of this approach looks bright. There are many avenues that can still be explored to describe more types of moduli spaces and we have only started looking at applications of the Weil-Petersson density of states. I hope this new tool set will be of use to the Quantum gravity community and that it will bring us one step closer to the ever elusive Quantum Gravity theory.

References

[1] Kennedy C.J. Aeppli A. et al Bothwell, T. Resolving the gravitational redshift across a millimetre-scale atomic sample. *Nature*, 602:420–424 (2022), February 2022. URL: https://doi.org/10.1038/s41586-021-04349-7.

[2] D. Hanneke, S. Fogwell Hoogerheide, and G. Gabrielse. Cavity control of a single-electron quantum cyclotron: Measuring the electron magnetic moment. *Phys. Rev. A*, 83:052122, May 2011. URL: https://link.aps.org/doi/10.1103/PhysRevA.83.052122, doi:10.1103/PhysRevA.83.052122.

[3] Julian Schwinger. Quantized gravitational field. *Phys. Rev.*, 130:1253–1258, May 1963. URL: https://link.aps.org/doi/10.1103/PhysRev.130.1253, doi:10.1103/PhysRev.130.1253.

[4] Assaf Shomer. A pedagogical explanation for the non-renormalizability of gravity, 2007. arXiv:0709.3555.

[5] John F. Donoghue. Gravitons and pions. *The European Physical Journal A*, 56(3), mar 2020. URL: https://doi.org/10.1140%2Fepja%2Fs10050-020-00091-2, doi:10.1140/epja/s10050-020-00091-2.

[6] Silk J Ellis, G. Scientific method: Defend the integrity of physics. *Nature*, 516:321–323, December 2014. URL: https://doi.org/10.1038/516321a.

[7] Roman Jackiw. Lower dimensional gravity. *Nuclear Physics B*, 252:343–356, 1985. URL: https://www.sciencedirect.com/science/article/pii/0550321385904481, doi:https://doi.org/10.1016/0550-3213(85)90448-1.

[8] Claudio Teitelboim. Gravitation and hamiltonian structure in two spacetime dimensions. *Physics Letters B*, 126:41–45, 1983. URL: https://www.sciencedirect.com/science/article/pii/0370269383900126, doi:10.1016/0370-2693(83)90012-6.

[9] Timothy Budd. Lessons from the mathematics of two-dimensional euclidean quantum gravity, 2022. URL: https://arxiv.org/abs/2212.03031, doi:10.48550/ARXIV.2212.03031.

[10] J. Bouttier. Matrix integrals and enumeration of maps, 2011. arXiv:1104.3003.

[11] Jason Miller and Scott Sheffield. Liouville quantum gravity and the brownian map i: The qle(8/3,0) metric, 2019. arXiv:1507.00719.

[12] Davood Momeni and Phongpichit Channuie. Exact solutions of (deformed) jackiw–teitelboim gravity. *The European Physical Journal C*, 81(6), jun 2021. URL: https://doi.org/10.1140%2Fepjc%2Fs10052-021-09327-x, doi:10.1140/epjc/s10052-021-09327-x.

[13] Maryam Mirzakhani. *Weil-Petersson volumes and intersection theory on the moduli space of curves*. J. Amer. Math. Soc., 20(1):1–23 (electronic), 2007.

[14] Yusuke Kimura. JT gravity and the asymptotic weil–petersson volume. *Physics Letters B*, 811:135989, dec 2020. URL: https://doi.org/10.1016%2Fj.physletb.2020.135989, doi:10.1016/j.physletb.2020.135989.

[15] B.H. Bowditch and D.B.A. Epstein. Natural triangulations associated to a surface, 1988. URL: https://www.sciencedirect.com/science/article/pii/0040938388900080, arXiv:math/0403247.

[16] Yi Huang. Mirzakhani's recursion formula on weil-petersson volume and applications, 2015. URL: https://arxiv.org/abs/1509.06880, doi:10.48550/ARXIV.1509.06880.

[17] Yi Huang. Mirzakhani's recursion formula on weil-petersson volume and applications, 2015. arXiv:1509.06880.

[18] Herbert S. Wilf. *generatingfunctionology*. AK Peters/CRC, 2005.

[19] L. Chekhov and R. C. Penner. On quantizing teichmüller and thurston theories, 2004. arXiv:math/0403247.

[20] Leonid O. Chekhov. Fenchel–nielsen coordinates and goldman brackets, 2020. URL: https://arxiv.org/abs/2008.12777, doi:10.48550/ARXIV.2008.12777.

[21] R. C. Penner. Weil-petersson volumes, 1992. URL: https://doi.org/10.4310/jdg/1214448257, arXiv:math/0403247.

[22] M Mirzakhani. Simple geodesics and weil-petersson volumes of moduli spaces of bordered riemann surfaces, 2007. URL: https://link.springer.com/article/10.1007/s00222-006-0013-2#citeas, doi:10.48550/ARXIV.2212.03031.

[23] Sedgewick R. Flajolet, P. *Analytic Combinatorics*. Cambridge: Cambridge University Press, 2009. doi:10.1017/CBO9780511801655.